ARL-TR-7790 ● SEP 2016

US Army Research Laboratory

Quasi-Steady Simulations for the Efficient Generation of Static Aerodynamic Coefficients at Subsonic Velocity

by Sidra I Silton

NOTICES

Disclaimers

ARL-TR-7790 ● SEP 2016

US Army Research Laboratory

Quasi-Steady Simulations for the Efficient Generation of Static Aerodynamic Coefficients at Subsonic Velocity

by Sidra I Silton

Weapons and Materials Research Directorate, ARL

REPORT DOCUMENTATION PAGE

Form Approved
OMB No. 0704-0188

1. REPORT DATE ***(DD-MM-YYYY)*** September 2016	**2. REPORT TYPE** Technical Report	**3. DATES COVERED (From - To)** December 2014–April 2015

4. TITLE AND SUBTITLE
Quasi-Steady Simulations for the Efficient Generation of Static Aerodynamic Coefficients at Subsonic Velocity

5a. CONTRACT NUMBER

5b. GRANT NUMBER

5c. PROGRAM ELEMENT NUMBER

6. AUTHOR(S)
Sidra I Silton

5d. PROJECT NUMBER
AH80

5e. TASK NUMBER

5f. WORK UNIT NUMBER

7. PERFORMING ORGANIZATION NAME(S) AND ADDRESS(ES)
US Army Research Laboratory
ATTN: RDRL-WML-E
Aberdeen Proving Ground, MD 21005-5069

8. PERFORMING ORGANIZATION REPORT NUMBER
ARL-TR-7790

9. SPONSORING/MONITORING AGENCY NAME(S) AND ADDRESS(ES)

10. SPONSOR/MONITOR'S ACRONYM(S)

11. SPONSOR/MONITOR'S REPORT NUMBER(S)

12. DISTRIBUTION/AVAILABILITY STATEMENT
Approved for public release; distribution is unlimited.

13. SUPPLEMENTARY NOTES

14. ABSTRACT

A quasi-steady sweep procedure that allows determination of the static aerodynamic coefficients for a range of angles of attack in a single simulation is extended to subsonic Mach numbers. Given a steady-state solution, the procedure can be used to generate multiple numerical simulations over a select range of angles of attack for a given set of flight conditions using the time-accurate Reynolds-Averaged Navier–Stokes equations. Computational Fluid Dynamics simulations are completed for a canard-controlled, fin-stabilized projectile at Mach 0.65 for a moderate range of angles of attack using a quasi-steady sweep procedure. Separate steady-state solutions are also computed at various angles of attack for comparison. Comparison of the results showed that the quasi-steady sweep procedure can provide accurate static aerodynamic coefficients efficiently if convergence at each time step is ensured.

15. SUBJECT TERMS
sweep procedure, Highly Maneuverable Airframe, rapid aerodynamic generation, Computational Fluid Dynamics, static aerodynamic coefficients

16. SECURITY CLASSIFICATION OF:			**17. LIMITATION OF ABSTRACT**	**18. NUMBER OF PAGES**	**19a. NAME OF RESPONSIBLE PERSON** Sidra I Silton
a. REPORT Unclassified	**b. ABSTRACT** Unclassified	**c. THIS PAGE** Unclassified	UU	54	**19b. TELEPHONE NUMBER (Include area code)** 410-306-0792

Standard Form 298 (Rev. 8/98)
Prescribed by ANSI Std. Z39.18

Contents

List of Figures

List of Tables

9999333

Acknowledgments

The author would like to thank the following:

- Dr James DeSpirito, US Army Research Laboratory (ARL) Flight Sciences Branch, for multiple conversations relating to the computational fluid-dynamics simulations
- The US Department of Defense (DOD) High-Performance Computing Modernization Program at the ARL Department of Defense Supercomputing Resource Center (DSRC), Aberdeen Proving Ground, Maryland, and at the US Air Force Research Laboratory DSRC, Wright–Patterson Air Force Base, Ohio, for the grant of high-performance computing time
- Mr Prasanth Kachgal, Metacomp Technologies, for multiple discussions to correctly implement the quasi-steady sweep procedure within CFD^{++}

1. Introduction

An accurate understanding of fundamental flow physics and accurate prediction of aerodynamic coefficients is critical to the development of precision munitions (Fresconi et al. 2011; Coyle and Silton 2015; Silton and Fresconi 2015). The flow fields associated with precision munitions can be very complex, involving shock-boundary layer interaction, unsteady wakes, and body, canard and tail-fin interactions (Sahu 1990; DeSpirito et al. 2003; Silton 2005; DeBonis et al. 2012; Bhagwandin 2014, 2015; Scheuermann et al 2015; Silton and Coyle 2015; Silton and Fresconi 2015). Simple empirical and analytical techniques such as PRODAS (Arrow Tech Associates 2015), Missile Datcom (Rosema et al. 2011), MISL3 (Lesieutre et al. 2002), and AP09 (Moore and Moore 2008) are not always able to accurately determine the complex 3-D flow interactions and associated nonlinear flow physics. Computational Fluid Dynamics (CFD) offers an alternative to compute these nonlinear interacting flow fields, providing detailed understanding of the associated nonlinear aerodynamic processes and predicting the associated aerodynamic coefficients that are required to determine if performance requirements can be met. CFD has continued to emerge as a critical technology for the aerodynamic design and assessment of flight vehicles. Bringing CFD into the earlier stages of design and development is necessary for it to be more effective; to bring CFD into the earlier stages, though, the results must be obtained as quickly and accurately as possible. However, even with the advancement of high-performance computing, CFD computing time is still much greater than the time required to obtain solutions using engineering-level codes. This means that CFD is not implemented until further along in the process, often after a problem is discovered.

Steady-state and/or time-accurate CFD methods can be used to obtain a complete set of aerodynamic coefficients (static coefficients and dynamic derivatives) in all flight regimes, from subsonic to supersonic speeds. In general, most of the aerodynamic coefficients of a projectile or missile in the supersonic regime can be generated efficiently using steady-state methods; only pitch damping may need to be calculated in a time-accurate manner. Time-accurate methods are sometimes required to accurately predict base flows and dynamic derivatives of these munitions, especially in the subsonic and transonic flight regimes (Oktay and Akay 2002; Park and Kwon 2003; DeSpirito and Heavey 2004; Murman 2007; DeSpirito and Plostins 2007; DeSpirito 2008; DeSpirito et al. 2009; Silton 2011; Da Ronch et al. 2012; Bhagwandin 2012; Klatt et al. 2012; Bhagwandin and Sahu 2014). The static aerodynamic coefficients can be obtained from a steady-state method. A number of researchers (Weinacht and Sturek 1990; DeSpirito et al. 2009;

Bhagwandin and Sahu 2014) found the pitch-damping coefficient derivative could also be determined using a steady-state coning methodology. More recent advances in computational modeling have also led to coupling of CFD codes to rigid-body dynamics (RBD) codes for the time-accurate simulation of free-flight motion, which allows determination of both the static aerodynamic coefficients and dynamic derivatives using the same numerical simulation (Sahu 2004; Costello et al. 2007; Sahu 2008; Sahu 2009; Stahl et al. 2009; Montalvo and Costello 2010; Sahu 2011; Camargo et al. 2012; Sahu and Fresconi 2015; Wang et al. 2015).

When designing a new precision munition, especially in the early stages, it is the static aerodynamic coefficients that are of greatest importance to ensure the munition can meet its range and maneuverability requirements. This requires the development of an aerodynamic database that likely includes a range of angles of attack and either roll angles or side-slip angles at a given (or multiple) Mach number(s). While the new coupled CFD–RBD method would require fewer total simulations, it is quite time intensive as it must be solved using the time-dependent Reynolds-Averaged Navier–Stokes (RANS) equations with very small time steps to accurately capture the flow physics. The traditional steady-state solution uses the same governing RANS equations, but allows for larger time steps to more quickly converge the solution. However, a large number of these steady-state solutions would be required to generate the aerodynamic database when nonlinear aerodynamic behavior is present (canard stall, vortex interactions, etc.) in the range of angle of attack of interest causing this method to be time intensive as well.

Recently, Sahu and Heavey (2010) demonstrated an alternative method for rapid determination of static aerodynamic coefficients using the time-accurate RANS equations; a quasi-steady sweep procedure that allows determination of the coefficients for an entire range of angles of attack. Although their research was on a complex nonaxisymmetric missile configuration, it was limited to the transonic and supersonic flight regimes. The work presented in this paper extends their work to the subsonic regime. Numerical computations using the quasi-steady sweep procedure are performed at Mach 0.65 on the high-maneuverability airframe (HMA) being developed at the US Army Research Laboratory (ARL) as a demonstrator platform for the precision-munitions research area (Fresconi et al. 2011; Silton and Fresconi 2013; Fresconi et al. 2014; Silton et al. 2014). Steady-state simulations were also performed for comparison with the sweep results. Computational resource requirements are included to show the efficiency of the quasi-steady sweep procedure.

2. Solution Technique

The commercially available code CFD^{++} v12.1.1 (Metacomp Technologies 2011), by Metacomp Technologies, Inc., is used for the CFD simulations. CFD^{++} is a finite-volume, unstructured solver capable of computing CFD solutions for a wide range of aerospace applications. In this study, CFD^{++} is used in both its steady-state and time-accurate modes to numerically solve the 3-D, compressible RANS equations to compute the flow solution.

The Goldberg 3-equation k-ε-R_t turbulence model (Goldberg et. al. 1998) was implemented in this study based on the findings by Silton and Fresconi (2013). This 3-equation model solves the transport equations for undamped eddy viscosity, R_t, in addition to turbulent kinetic energy (k) and its dissipation rate (ε). This solution methodology accounts for nonequilibrium conditions and avoids free-stream-turbulence decay under shear-free flow conditions. For the current problem, initialization of the turbulence transport was completed by setting the turbulence intensity to 2% and the turbulent-to-molecular viscosity ratio to 50, as the length scale was not known.

2.1 Steady-State Simulation

The flow solution was advanced toward steady-state convergence using a point-implicit time-integration scheme with local time-stepping, defined by the Courant–Friedrichs–Lewy (CFL) number. A linear ramping schedule was used to gradually increase the CFL number over the first 100 iterations after which the CFL remained constant until convergence was reached. As only the subsonic flight regime ($0.3 < M < 0.8$) is considered in this paper, the suggested CFL ramping is from 1 to 100. Depending on the angle of attack being investigated, the maximum CFL number for the ramping was limited to 25 or 50. The multigrid W-cycle method with a maximum of 4 cycles and 20 coarse grid levels was used to accelerate convergence. Implicit temporal smoothing was applied for increased stability, which is especially useful where strong transients arise. The spatial discretization function was a second-order, upwind scheme using a Harten–Lax–van Leer-Contact (commonly, HLLC) Riemann solver and Metacomp's multidimensional Total-Variation-Diminishing (commonly, TVD) flux limiter (Metacomp Technologies 2011). Double-precision format was used for all computations.

Solution convergence (typically within 3,000 iterations) was determined by 1) a several-orders-of-magnitude reduction of the cell-averaged residuals of the RANS equations until the residuals plateaued and 2) the total, tail-fin, and canard forces and moments reaching asymptote and unchanging to within 0.1%.

2.2 Quasi-Steady Sweep Simulation

Using the equivalent of a series of steady-state simulations, the flow solution for the quasi-steady sweep is generated using the CFD solver's time-accurate mode to obtain the static aerodynamic coefficients across a range of angles of attack in a single numerical simulation. The time-accurate mode utilizes the implicit solver with dual time-stepping. Dual time-stepping employees 2 time-steps; an "outer" or global time-step that corresponds to the time discretization of the physical time variation and an "inner" or local time variation that helps to satisfy the physical transient equations.

The "outer" time-step is chosen to provide the desired time accuracy and is applied to every cell. Typically, this is set to a small value to ensure that the flow features are sufficiently resolved in time. In the present, sweep simulation, the time-accurate, dual time-step method is used to determine a "quasi-steady" solution at each time-step, which corresponds to an increment of rotation, in an efficient manner. Therefore, a large global time-step of 1.0 s is employed. This large time-step drives the rate of change of the flow variables with respect to angle of attack to zero as quickly as possible. Thus, the solutions are not transient, as is typical of a time-accurate simulation, but rather multiple static solutions.

The "inner" time-step is determined internal to the solver via the CFL number that is equal to the final maximum CFL number from the steady-state solution. The inner time-step (or iteration) is a local, nonphysical time-step used to converge the time-accurate RANS equations at each physical time-step. The time-step for the inner iteration is allowed to vary spatially. For the inner iteration, the multigrid W-cycle method and implicit temporal smoothing are applied to accelerate convergence of the inner iterations and therefore the outer global time-step. If the inner iterations are not sufficiently converged, the solution is not converged and there is a loss in accuracy. The number of inner iterations is chosen such that approximately a 2-order-of-magnitude reduction in the cell-averaged "inner" residuals was achieved. Typically, 100 inner iterations are found to be adequate in the present simulations using the quasi-steady sweep procedure. These requirements are significantly larger than for a "standard" time-accurate solution where only 5–20 inner iterations are required for a 1–2-order-of-magnitude drop in the cell-averaged inner residuals and a converged solution.

The steady-state solution with the mesh rotated to the lowest desired angle of attack serves as the initial condition for the initial sweep solution. For each step of the sweep solution, the computational grid is rotated by a small increment and a new solution is computed. In CFD^{++}, the rotation takes place at the end of the time-step; the first time-step is solved at the starting angle of attack. This process continues across the desired range of angles of attack. Figure 1 shows the location of the body at various stages of the sweep. In this example, the rotation point is at the projectile's center of gravity. The rotation angle must be chosen small enough to capture any nonlinear aerodynamic effects that may be present. In the present sweep simulations, a rotation-angle increment of 0.25° was able to suitably capture the nonlinear aerodynamic effects.

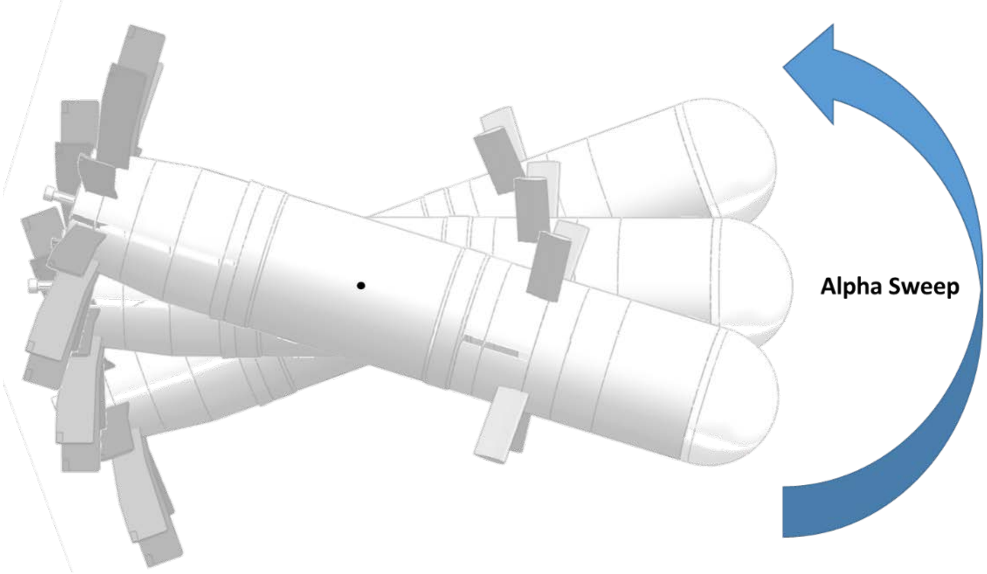

Fig. 1 **Location of the projectile at various stages of the sweep procedure**

Every numerical solver has its nuances in how the sweep procedure is implemented. Details of implementation of the quasi-steady sweep simulations in CFD^{++} can be found in the Appendix.

3. Geometry

3.1 Model Geometry

The geometry utilized for this study was the HMA designed as the platform to demonstrate advanced guided munitions using low-cost technologies. Both the body–fin configuration (BF) and the body–fin–canard configuration were considered (Fig. 2).

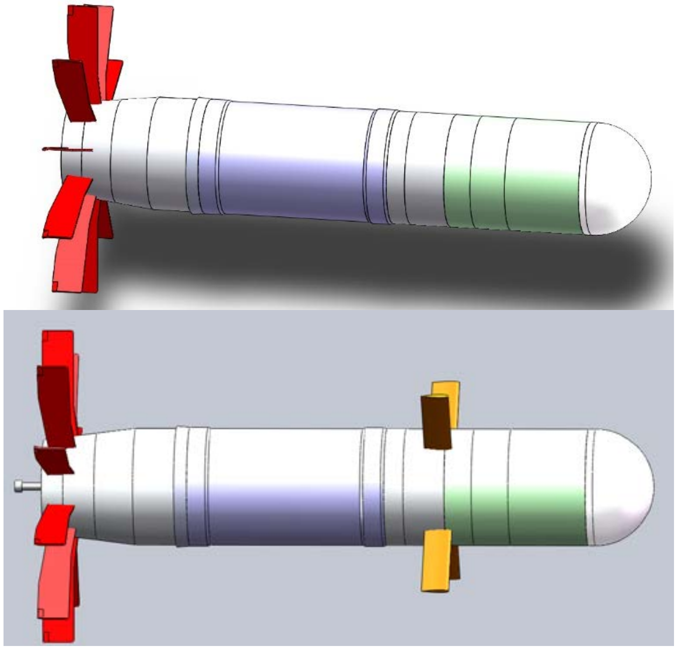

Fig. 2 **Subsonic geometries: BF (top) and body–fin–canard configuration (bottom)**

The geometric model was created in SolidWorks (Dassault Systemes 2012) and has a body reference diameter of 83 mm (1 caliber). This was a simplified geometry with the gaps and slots in the body needed to accommodate the tail fins suppressed. The body geometry consisted of a hemispherical nose cap; a nearly cylindrical body 320.38 mm (3.86 cal.) long; and a 66.4-mm (0.8-cal)-long, 7° boattail. The overall projectile length was 427.23 mm (5.15 cal.). Ten flat-plate fins having a span of 217.22 mm and an average chord of 20.5 mm, with the trailing edge located 4.48 mm from the base of the projectile, were included for stability. The tail fins were shaped such that they can store flush in the body for gun launch while maximizing area for stability. A 7-mm-high, 3.8-mm-deep tab at the tip of each tail fin was bent at a 15° angle such that the projectile would roll clockwise (looking from rear of airframe).

For the body–fin–canard configuration, 4 NACA0015 airfoils, rotated 45° off plane, were added to the model. Each of the 4 canards had a chord of 18.86 mm and a semispan of 96.36 mm with the quarter chord located 144.7 mm aft of the nose of the projectile. Canard deflection angles of 0° and 4° pitch up about the quarter chord were considered. For simplicity, the model had the canards directly attached to the body; the body slots were suppressed.

3.2 Numerical Grids

The grids used in the numerical simulation were created with MIME v4.1 by Metacomp Technologies (Metacomp Technologies 2010). MIME is an unstructured mesh generator that allows triangular or quadrilateral dominant cells for the surface mesh. Once an adequate surface mesh is generated, prism layers can be specified and created when the volume mesh (tetrahedral dominant) is generated.

Figure 3 shows the extent of the outer boundary. It extended approximately 35 body lengths from the projectile in all directions. Cylindrical density boxes were placed in the wake of the projectile and tail fins to ensure proper resolution in this area. An additional density box (No. 3) was placed between the canards and the tail fins, when the canards were present, to ensure the canard-tip vortices would not dissipate significantly due to mesh resolution prior to reaching the tail fins. The surface mesh and boundary-layer growth was restricted to a ratio of 1.2 or less. The growth ratio was relaxed to 2.0 when creating the remainder of the volume mesh. The prism-layer spacing was chosen such that wall-function spacing (nondimensional wall distance, $30 \leq y^{+} \leq 60$) was present on the body, while a solve-to-wall mesh $y^{+} \approx 1$ was used on and around the tail fins and canards. To achieve this, a first cell spacing for the prism layer was specified at 3.5×10^{-3} mm on the tail fins and canards, 0.25 mm on the body, and 0.2 mm on the nose. This produced $y^{+} \approx 1$ on the tail fins and canards as well as on the body immediately surrounding them. On the nose of the airframe and remainder of the body, the y^{+} varied between 25 and 45. MIME allowed for a smooth transition between the specified spacings. Mesh-refinement studies, which showed that this mesh achieved grid independence, have been conducted for this body–fin geometry (Silton and Fresconi 2013) and are not included in this paper. Mesh-refinement studies for the body–fin–canard geometry have not yet been completed. The computational domain is fully 3-D with no symmetry. The body–fin mesh consisted of approximately 26 million cells, while the body–fin–canard mesh consisted of approximately 45 million cells.

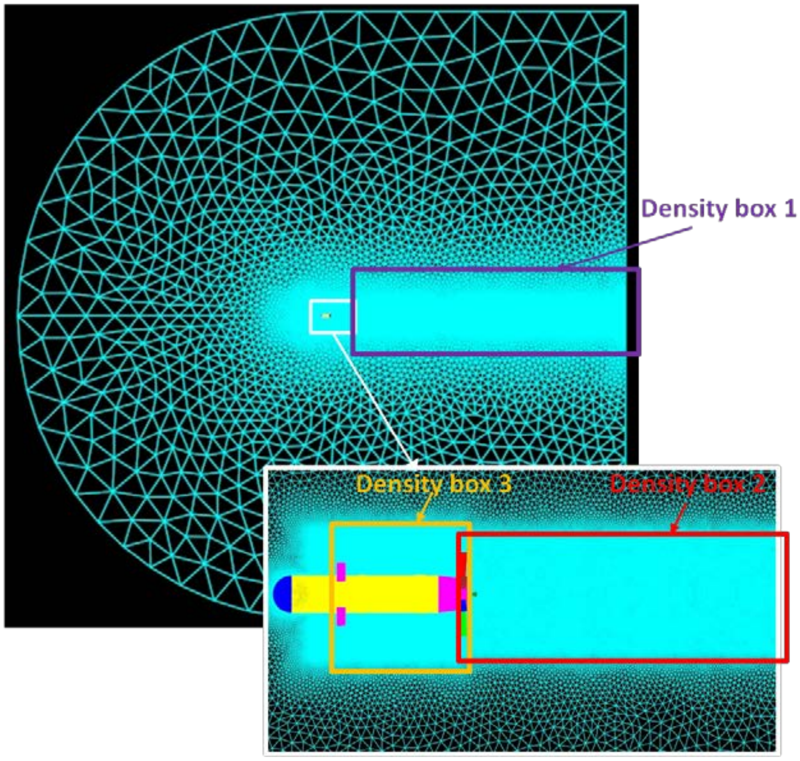

Fig. 3 Extent of outer mesh boundary with close-up of projectile showing locations of density boxes

3.3 Boundary Conditions

The entire far-field boundary was set as “characteristics-based” inflow/outflow. This boundary condition takes the specified free-stream conditions and solves a Riemann problem at the boundary using the supplied data as a virtual state outside the domain. The walls of the projectile were specified as an adiabatic, no-slip, viscous boundary. Wall functions were used to compute the boundary layer on the projectile’s surface except where there was adequate prism-layer resolution to solve to the wall, as was the case on the tail fins and canards.

4. Results and Discussion

Numerical simulations were performed to assess the ability and efficiency of the quasi-steady sweep procedure to predict the flow field and aerodynamic coefficients for a complex gun-launched-projectile configuration in the subsonic flight regime. All computations were completed using a free-stream temperature and pressure of 288.15 K and 101325 Pa, respectively. The study was conducted at Mach 0.65 (220 m/s). Angles of attack between –14° and 14°, inclusive, were considered. The flow domain was initialized using free-stream conditions everywhere.

4.1 Body–Fin Configuration

Steady-state simulations were completed for the BF at α = –14°, 0°, 2°, 3°, 5°, 8°, 10°, and 14°. The quasi-steady sweep procedure was performed using the steady-state solution at $\alpha = -14°$ as the initial condition. The critical parameters were varied to determine the requirements for an accurate solution. The critical parameters varied were CFL = 10 and 50; angle-of-attack increments ($d\alpha$) = 0.5°, 0.25°, and 0.1°; and number of inner iterations (N) = 50, 100, and 200.

4.1.1 CFL = 10

Initially, parameters were set to CFL = 10 (small CFL is typically warranted when determining time-accurate solutions) with 50 inner iterations (Sahu and Heavey 2010) and $d\alpha$ = 0.25° and 0.1° were investigated. Figure 4 shows the convergence history of the solution residual for the inner iterations as a function of the $d\alpha$ used. Both increments produce approximately 1-order-of-magnitude drop in residuals, although they do not level off as would be expected of a completely converged solution.

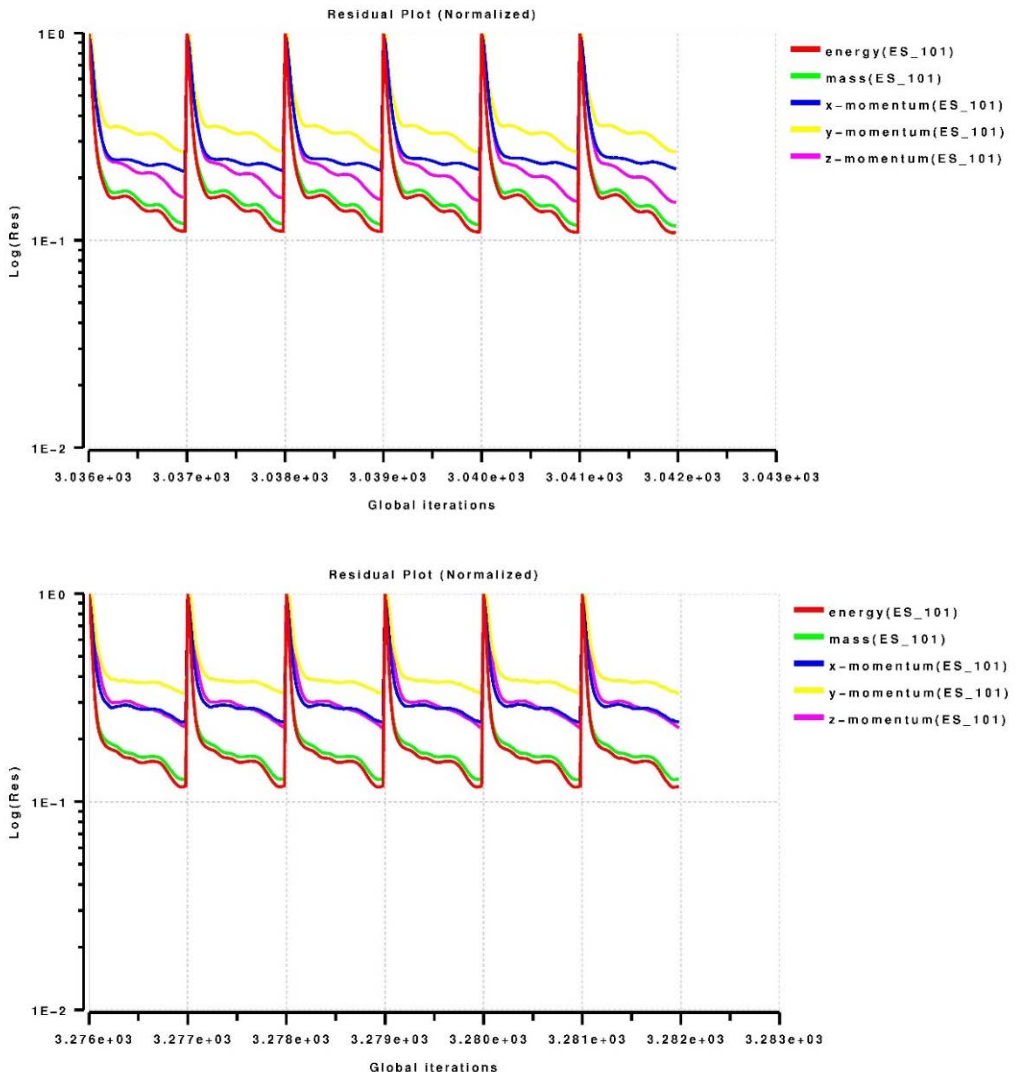

Fig. 4 Time history of solution residual as a function of $d\alpha$ for CFL = 10, N = 50; $d\alpha$ = 0.25° (top) and 0.1° (bottom)

Comparison of the resulting lift and drag coefficients (C_L and C_D, respectively) obtained from the quasi-steady sweep procedure to those obtained from the steady-state methodology were reasonable for both $d\alpha$ values. For the pitching moment, C_m, the results obtained from the sweep procedure showed reasonably good agreement between the 2 $d\alpha$ increments investigated. However, there are some very small differences between the steady-state values and the sweep values above $\alpha =$ 5° (Fig. 5) that are most noticeable in the fin component contribution. For the roll torque, C_{l_o}, there was good agreement between the steady-state results and the sweep procedure for $d\alpha = 0.1°$; agreement is not as good for the sweep procedure with $d\alpha = 0.25°$ (Fig. 6). The $d\alpha = 0.25°$ sweep results are not symmetric about $\alpha = 0°$ as is expected for this symmetric configuration. Therefore, the convergence of the inner iterations for $d\alpha = 0.25°$ was investigated.

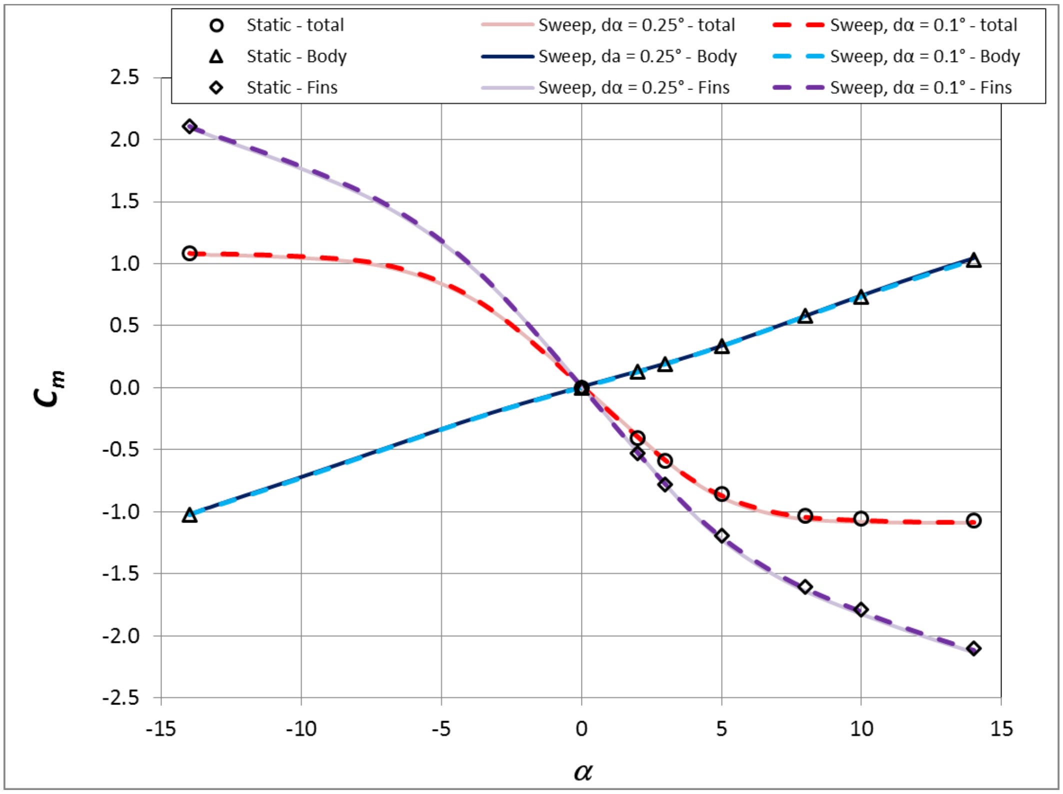

Fig. 5 Pitching-moment coefficient for BF comparing $d\alpha$ variation to steady-state results, CFL = 10 and N = 50

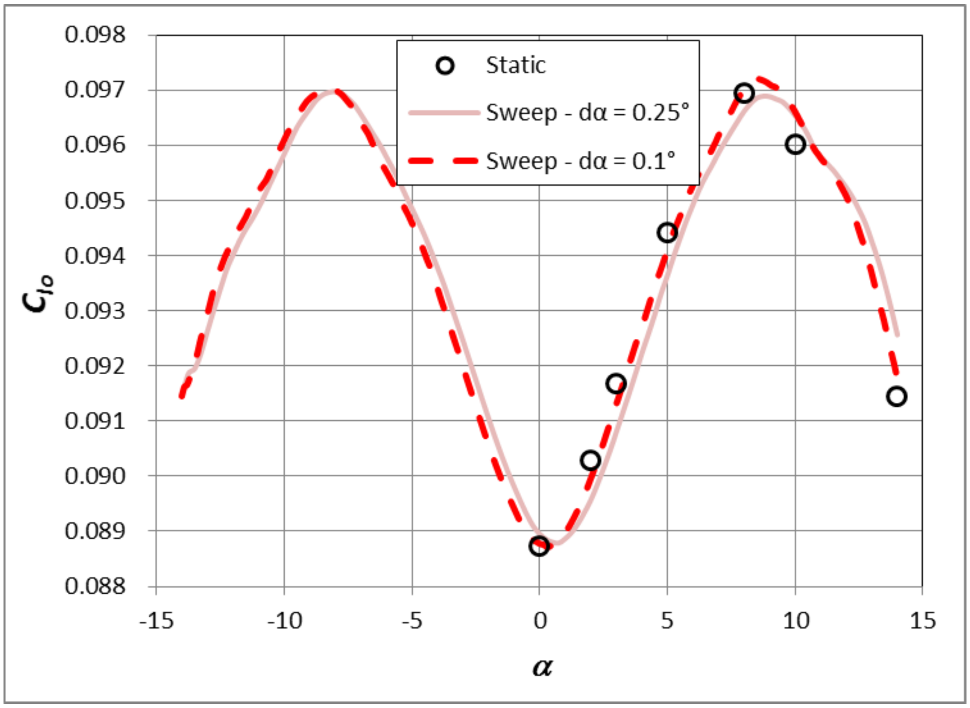

Fig. 6 Roll-torque coefficient for BF comparing $d\alpha$ variation to steady-state results, CFL = 10 and N = 50

As expected, increasing the number of inner iterations allowed further convergence in the solution residuals for the inner iterations (Fig. 7). Nearly 2-orders-of-magnitude drop are achieved for 200 inner iterations. With the improved convergence at each time step, a change in C_{l_o} over the first 40 steps of the sweep procedure can be seen (Fig. 8). Although the actual values do not change significantly (the scale is expanded), the shift to the left indicates a better solution can be achieved (similar to that of $d\alpha = 0.1°$) with an increase in the number of subiterations.

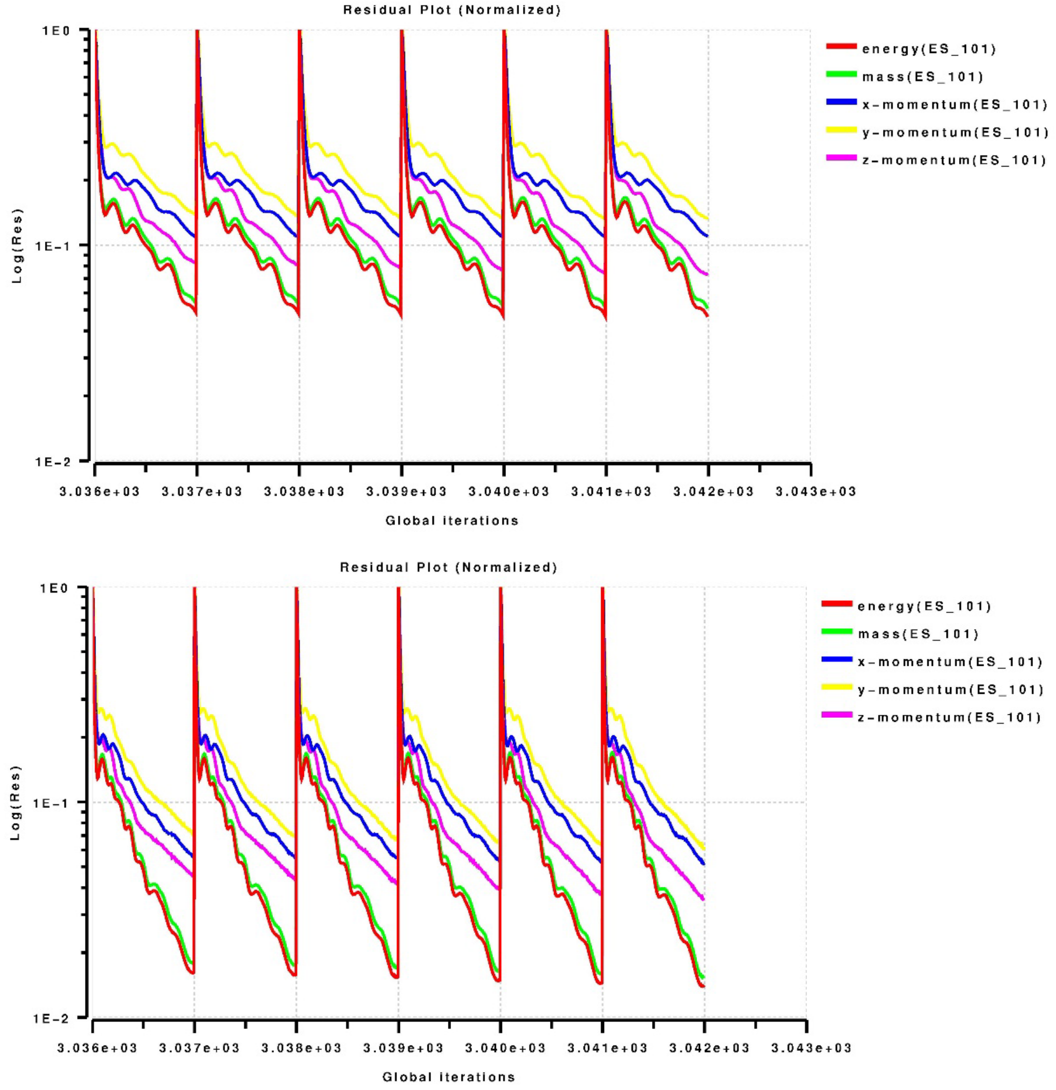

Fig. 7 Time history of solution residual as a function of number of inner iterations for CFL = 10, $d\alpha$ = 0.25°; N = 100 (top) and N = 200 (bottom)

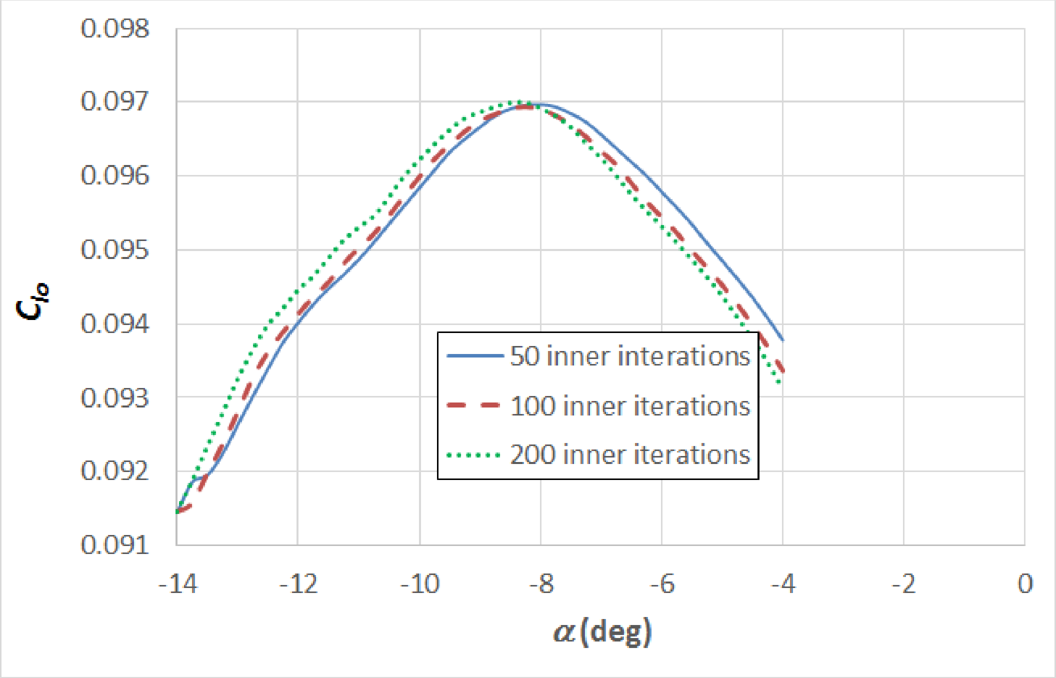

Fig. 8 Roll-torque coefficient for BF for varying number of inner iterations, CFL = 10 and $d\alpha$ = 0.25°

Using $d\alpha = 0.1°$ and N = 50 or $d\alpha = 0.25°$ and N = 200 both produce reasonable sweep results when compared with the steady-state solutions, in a reasonably efficient manner. All solutions were obtained using 256 central processing units (CPUs) on a SGI ICE X supercomputer. Each steady-state solution takes approximately 3.5 wall-clock h (2,000 iterations to converge, approximately 6 s per iteration). For $d\alpha = 0.25°$ and N = 200, it takes approximately 21 min per angle or 40 h for the entire sweep (10,000 CPU h). For $d\alpha = 0.1°$ and N = 50, this time was further reduced to 3.5 min per time-step or 15 h for the entire sweep (4,000 CPU h). Even assuming only 1° increments, it would take nearly 26,000 CPU h for the 29 steady-state solutions, thus realizing a CPU savings of up to 85% using the quasi-steady sweeps.

4.1.2 CFL = 50

After completing the sweep-procedure comparison for the BF with CFL = 10, it was determined the quasi-steady sweep procedure could be completed in a more efficient manner if a larger CFL value—similar to that used for the steady-state simulations—was chosen, rather than using a small CFL as would be the case if a truly time-accurate solution was being sought. Use of a larger CFL in a steady-state simulation typically allow convergence in fewer iterations. Since a quasi-steady sweep is solving for a "steady-state" solution at each time-step, it was thought that convergence at each time-step could be achieved with fewer inner iterations if a larger value for the CFL number was chosen. As the CFL number for some of the steady-state simulations at higher angles of attack had to be limited to 50 in order for convergence to be achieved for the BF (if a CFL greater than 50 was chosen, convergence was not possible), it was desirable to know the improved efficiency of sweep procedure and the required parameters if the CFL was set to 50 for the quasi-steady sweeps.

Because inner-iteration convergence is required to achieve accurate solutions, the number of inner iterations required for convergence at each $d\alpha$ (0.5°, 0.25°, and 0.1°) was investigated first. The findings for each $d\alpha$ were the same; there were small differences in force and moment coefficients when the results of N = 50 and N = 100, but virtually no differences when the results of N = 100 and N = 200 were compared.

The convergence history of the inner iterations for the $d\alpha = 0.25°$ case (Fig. 9) shows why this is the case. There is a decrease in the residuals during the inner iterations from approximately 2E-2 to 1E-2 when N = 100 is used rather than N = 50. When N is further increased to 200, the inner-iteration residuals plateau at 1E-2 indicating that the solution has converged. Thus, N = 100 was chosen for all $d\alpha$ investigated.

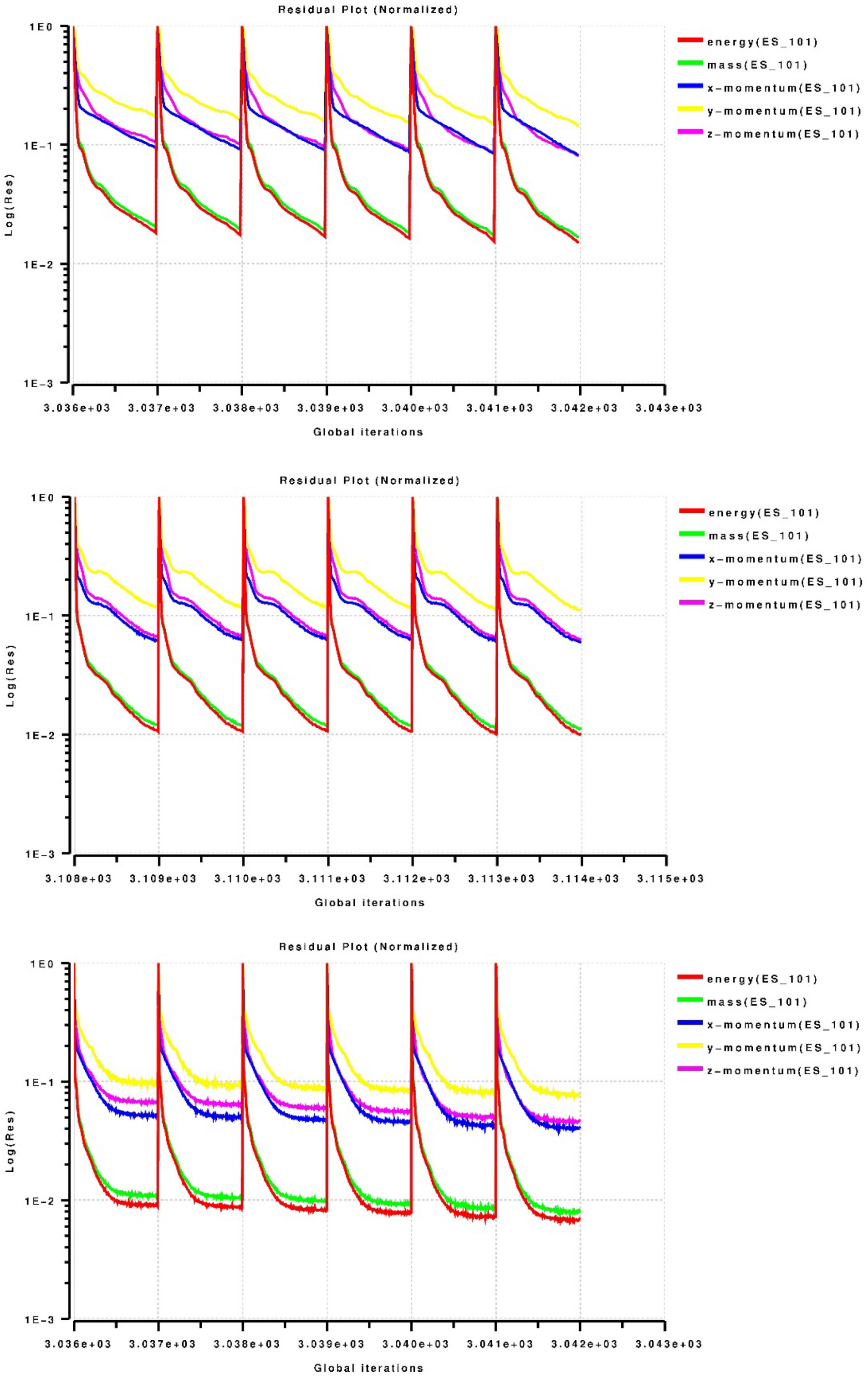

Fig. 9 Time history of solution residual as a function of number of inner iterations for CFL = 50, $d\alpha$ = 0.25°; N = 50 (top), N = 100 (middle), and N = 200 (bottom)

With inner iteration convergence achieved, the results of the quasi-steady sweep for $d\alpha = 0.5°$, $d\alpha = 0.25°$ and $d\alpha = 0.1°$ were compared. Most of the forces and moments for the total configuration, as well as the body component contribution and fin component contribution (C^F) were identical and in good agreement with the steady-state solutions. Figures 10–13 show the fin component contribution to the forces and moments for the sweep procedure. Only C_{l_o} shows any difference for $d\alpha = 0.5°$, and that is negligible even with the enlarged scale used. The total value of roll torque shown in Fig. 13 is equivalent to the fin component contribution as it is the only contribution.

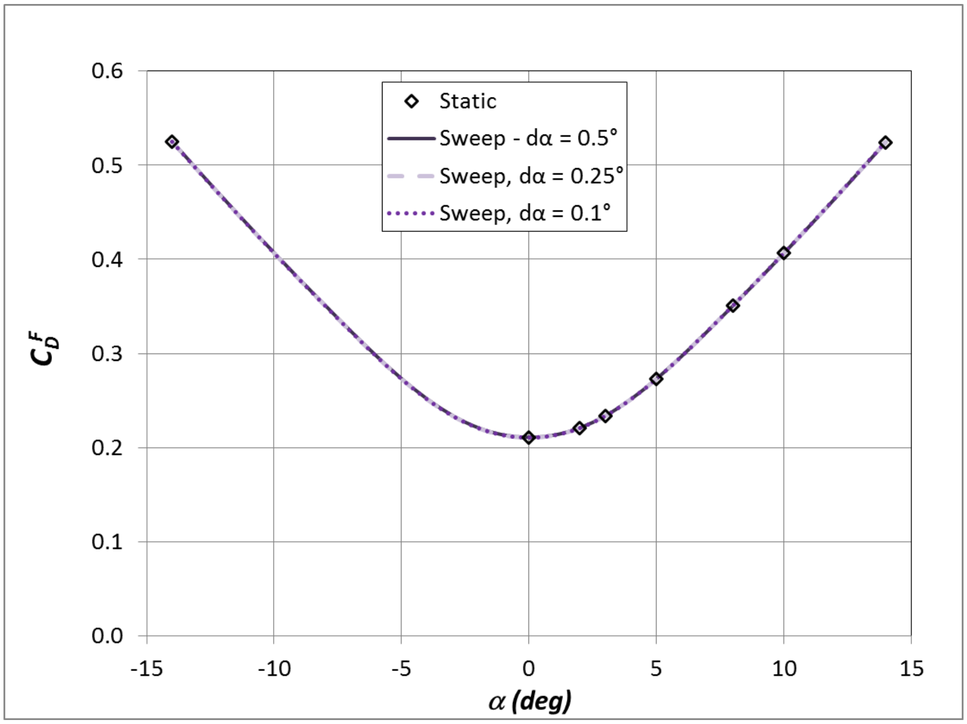

Fig. 10 Fin component contribution to drag coefficient for BF with CFL = 50, N = 100, $d\alpha$ comparison

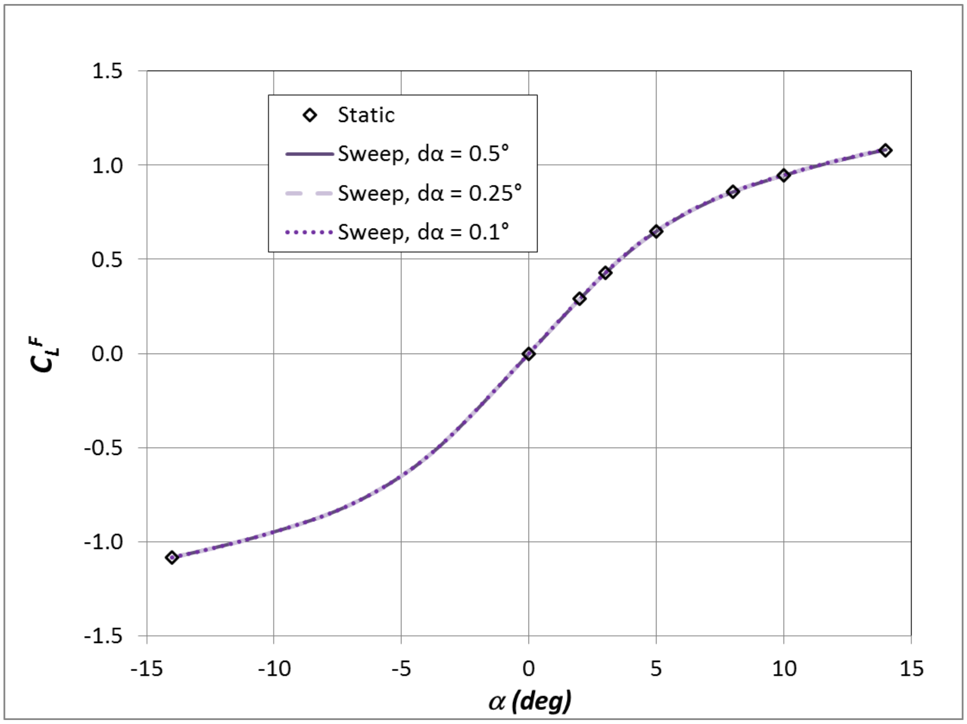

Fig. 11 **Fin component contribution to lift coefficient for BF with CFL = 50, N = 100, $d\alpha$ comparison**

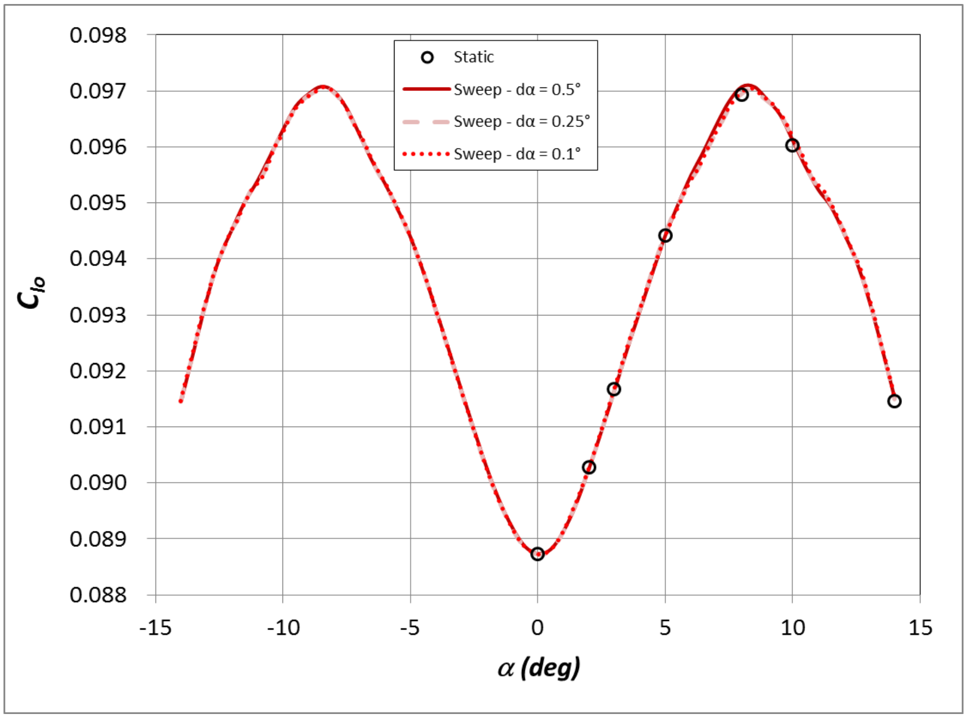

Fig. 12 **Roll-torque coefficient for BF with CFL = 50, N = 100, $d\alpha$ comparison**

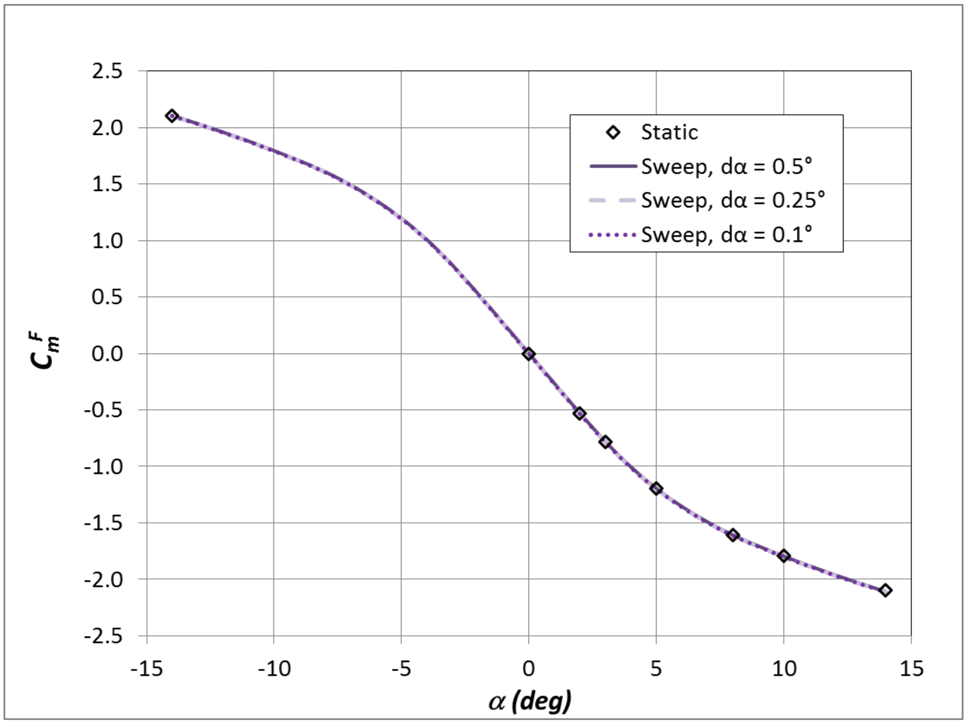

Fig. 13 Fin component contribution to pitching-moment coefficient for BF configuration with CFL = 50, N = 100, $d\alpha$ comparison

Figures 14–16 show the body component contribution (C^B) to the forces and moments for the sweep procedure. Roll-torque coefficient is not shown as the body does not contribute to that moment. Even using dα=0.5°, very good agreement with the steady-state solutions is achieved. Thus, agreement in the total forces and moments predicted using the sweep procedure and the steady-state solutions is achieved for all of the increments investigated, indicating that for the BF at subsonic velocity an increment as large as dα=0.5° is acceptable. This does, of course, assume a sufficient number of inner iterations is utilized. It becomes the researcher's choice of the desired increment, based on efficiency or resolution.

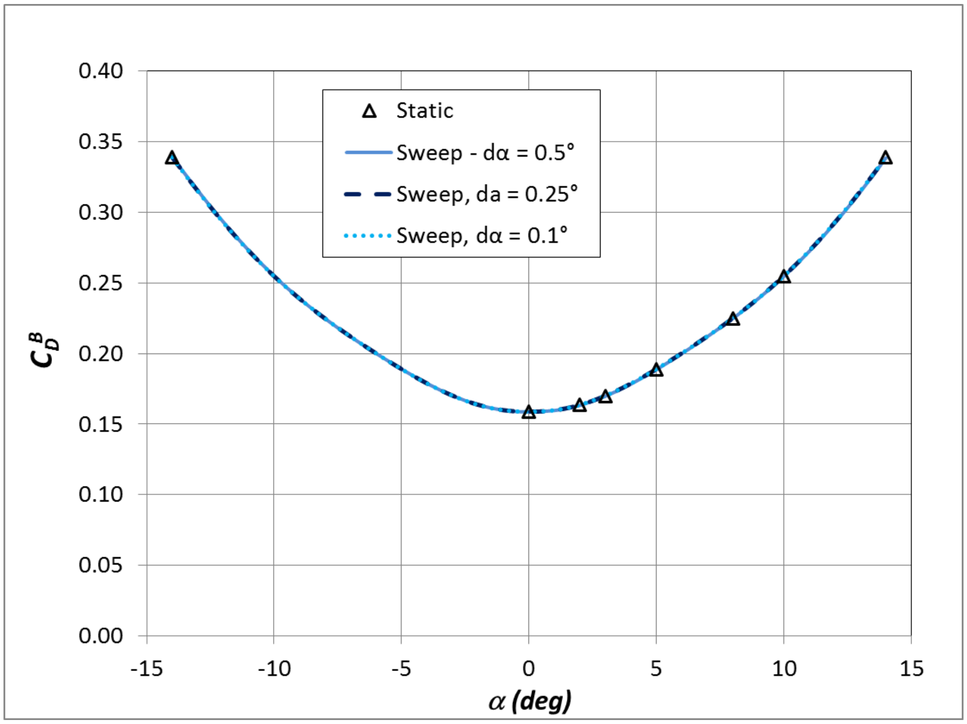

Fig. 14 **Body component contribution to drag coefficient for BF with CFL = 50, N = 100, $d\alpha$ comparison**

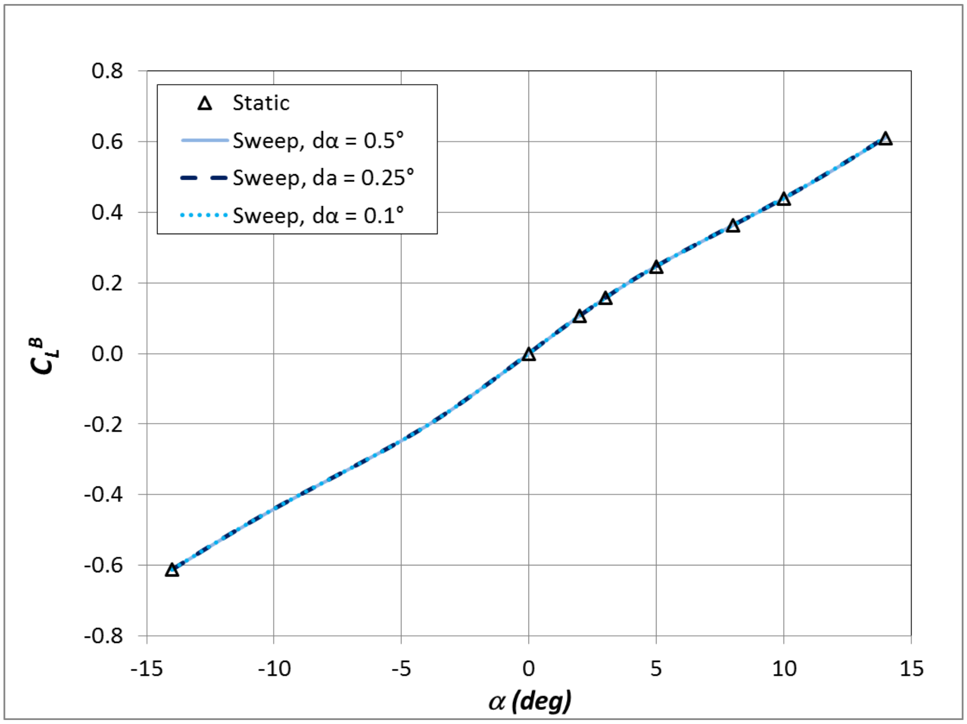

Fig. 15 **Body component contribution to lift coefficient for BF with CFL = 50, N = 100, $d\alpha$ comparison**

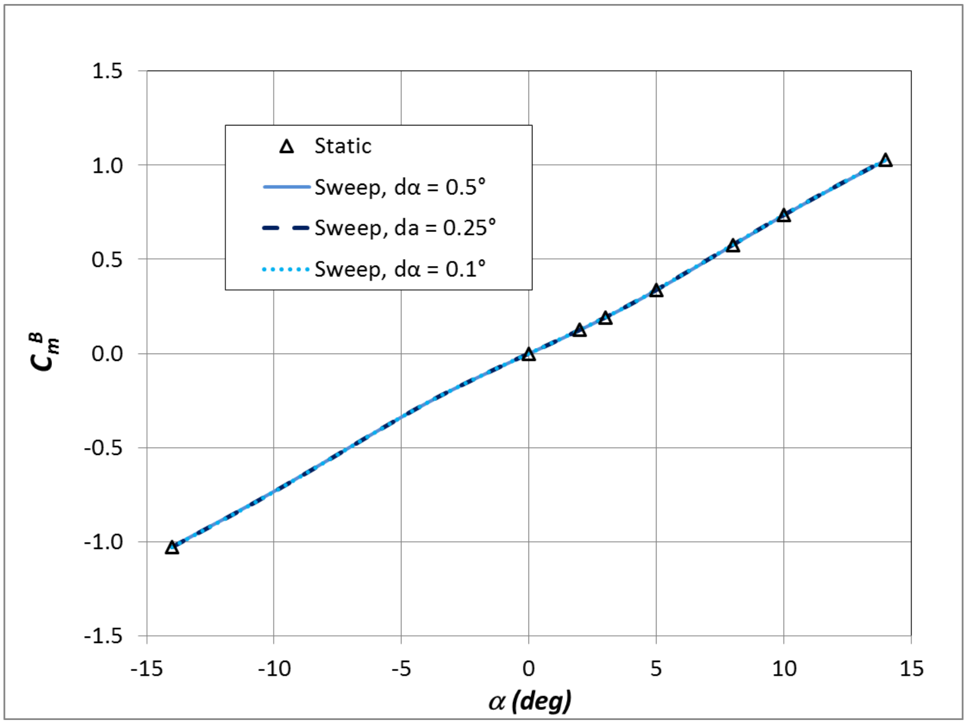

Fig. 16 Body component contribution to pitching-moment coefficient for BF with CFL = 50, N = 100, $d\alpha$ comparison

For $d\alpha = 0.5°$, N = 100, 11.7 wall-clock h on 256 cores of the SGI ICE X were required (2,995.2 CPU h total). For $d\alpha = 0.25°$, N = 100, 21.7 wall-clock h on 256 cores of the SGI ICE X were required (5,555.2 CPU h total). For $d\alpha = 0.1°$, N = 100, 51.9 wall-clock h on 256 cores of the SGI ICE X were required (13,286.4 CPU h total).

For the body–fin configuration, completing the quasi-steady sweep allows a range of angles of attack to be investigated in significantly less time than if individual steady-state simulations were used (see Table 1). When completing the quasi-steady sweep simulations, it is critical to ensure the inner iterations are converged. The number of inner iterations required to achieve convergence varies with CFL number as well as Mach number. The study conducted by Sahu and Heavy (2010) found only 25–50 inner iterations were required to achieve time-step convergence in the transonic and supersonic regimes. In the subsonic regime investigated here, 50–200 inner iterations were required depending on the CFL number chosen. For CFL = 10, the required number of inner iterations for convergence varied with $d\alpha$. Only 50 inner iterations were required for $d\alpha = 0.10°$, while 200 inner iterations were required for $d\alpha = 0.25°$. This meant the coarser angular resolution actually required more computational resources (Table. Additionally, inner-iteration convergence would need to be investigated each time a different angular resolution was desired if CFL = 10 was chosen. For CFL = 50, the required number of inner iterations for convergence (N = 100) did not vary with $d\alpha$. Choosing CFL = 50 ensures that once inner-iteration convergence is achieved at one angular resolution, changing the angular resolution does not vary those criteria. The computational requirement is directly proportional to your desired angular resolution.

Table 1 Comparison of time required to obtain converged solution for –14° ≤ α ≤ 14° at $d\alpha$ indicated

CFL	$d\alpha$ (°)	N	CPU hours
Steady-state	1.00	. . .	26,000
10	0.10	50	4,000
	0.25	200	10,000
50	0.10	100	13,286
	0.25	100	5,555
	0.50	100	2,995

4.2 Body–Fin–Canard

The body–fin–canard configuration is investigated for canards in the x-orientation only (i.e., 45° rotation out of the lift plane). The canards are considered in their undeflected position ($\delta = 0°$) as well as for a 4° deflection about its quarter chord for a pitch up maneuver ($\delta = 4°$). Two canard deflection angles were considered as it was unknown if variations in canard separation, canard stall, canard-root and/or -tip vortex shedding, and vortex–fin interactions due to canard deflection would require different values of the critical parameters of the sweep procedure to obtain agreement with the steady-state solutions.

As was done for the BF, steady-state simulations were completed first. The steady-state simulations were completed at $\alpha = 0°,\ \pm 2°,\ \pm 3°,\ \pm 5°,\ \pm 8°,\ \pm 10°$, and $\pm 14°$. The sweep procedure was performed using the steady-state solution at $\alpha = -14°$ as the initial condition. The critical parameters were varied to determine the requirements for an accurate solution. The critical parameters varied were CFL = 10 and 50; $d\alpha$ = 0.25°, 0.1°, and 0.05°; and N = 50, 100, and 200.

4.2.1 δ = 0°

As with the BF, the body–tail–canard configuration with the canards undeflected (BFC0), CFL = 10, N = 50 was investigated first for $d\alpha = 0.25°$ and $d\alpha = 0.1°$. CFL = 10 was considered for the BFC0 as the BFC0 quasi-steady sweeps were completed simultaneously with the quasi-steady sweeps for BF. The CFL = 10 results are presented for the BFC0 to further show the effects of not converging the inner iterations.

Inner-iteration convergence for the BFC0 was similar to that of the BF (Fig. 4). Agreement between the quasi-steady sweep procedure and steady-state results for the BFC0 for CFL = 10 were not as good as those of the BF, indicating inner-iteration convergence is even more important as the flow field becomes more complicated. Agreement was good for the lift and drag coefficients (Figs. 17 and 18, respectively). However, this is not the case for either C_m (Fig. 19) or C_{l_o} (Fig. 20); agreement was quite poor for $|\alpha| > 5°$, especially for $d\alpha = 0.25°$. While the discrepancies in C_{l_o} were also present in the BF, those in C_m were not. An examination of the component contributions to C_m shows the canard component contribution (C^C) is the cause of the discrepancy (Fig. 21). With the inner iterations not adequately converged, canard stall and separation are not properly predicted. Increasing N = 200 for $d\alpha = 0.25°$ produces results closer to those for $d\alpha = 0.1°$, N = 50 (Fig. 22), but at a significant time penalty.

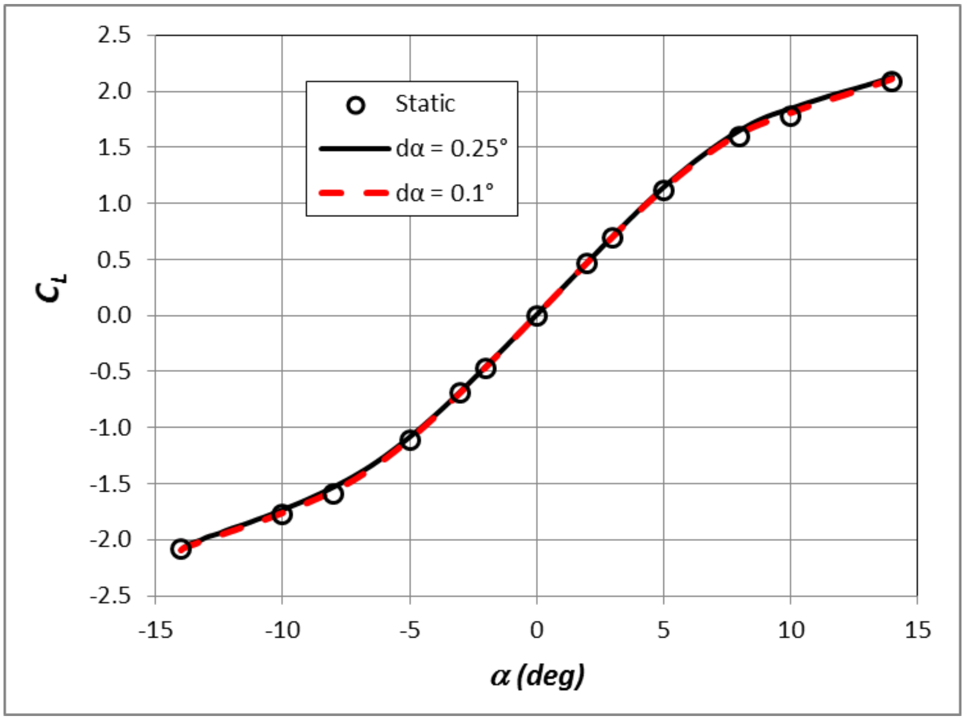

Fig. 17 Lift coefficient for BFC0 with CFL = 10, N = 50, $d\alpha$ comparison

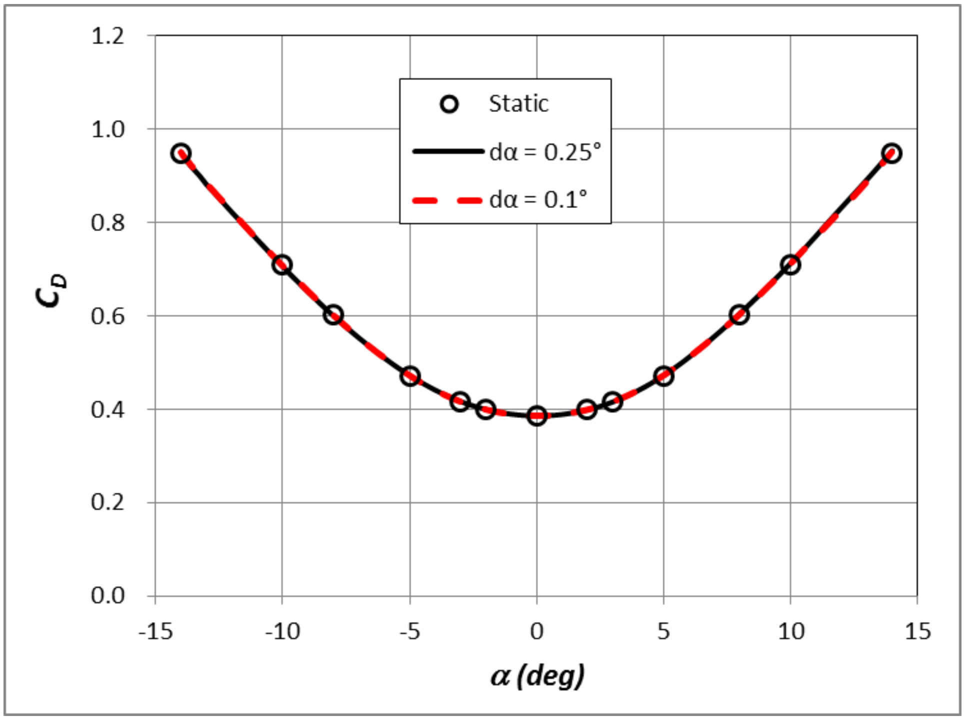

Fig. 18 Drag coefficient for BFC0 with CFL = 10, N = 50, $d\alpha$ comparison

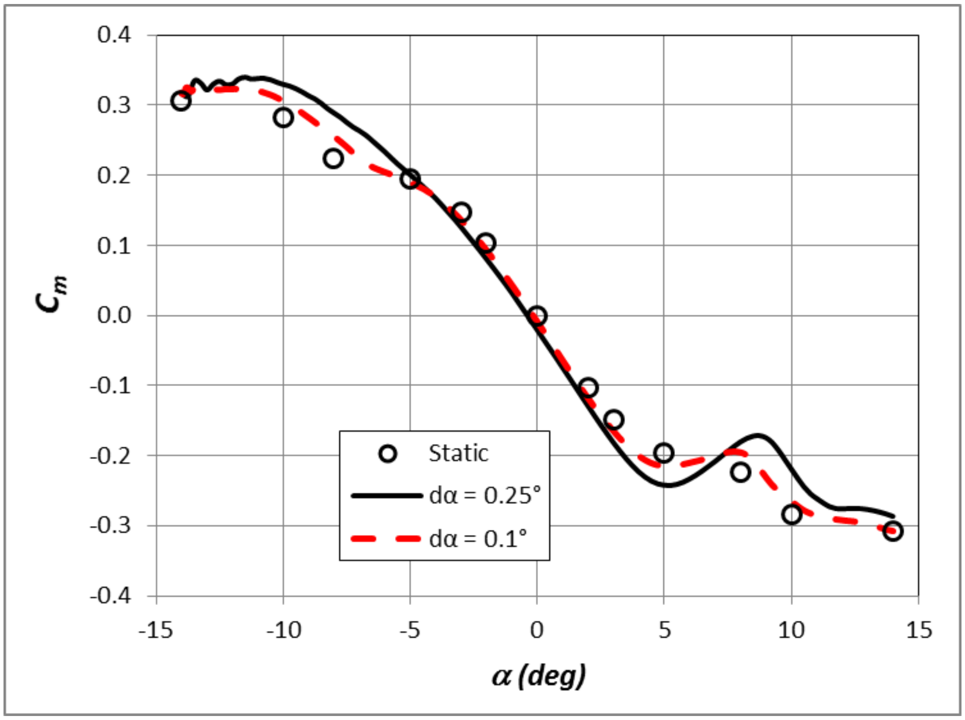

Fig. 19 Pitching-moment coefficient for BFC0 with CFL = 10, N = 50, $d\alpha$ comparison

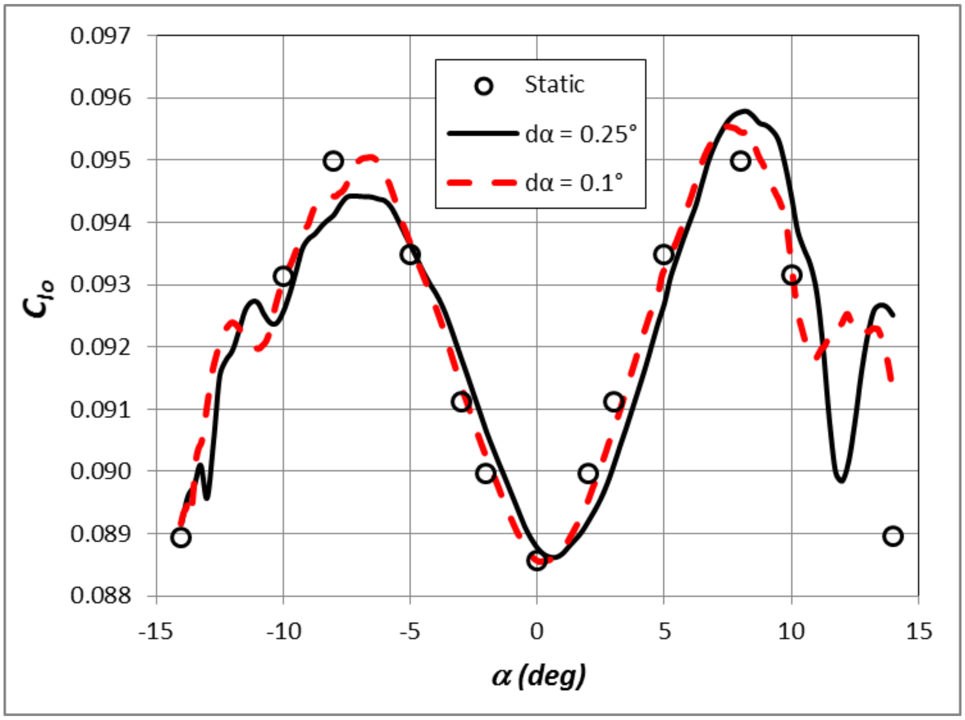

Fig. 20 Roll-torque coefficient for BFC0 with CFL = 10, N = 50, $d\alpha$ comparison

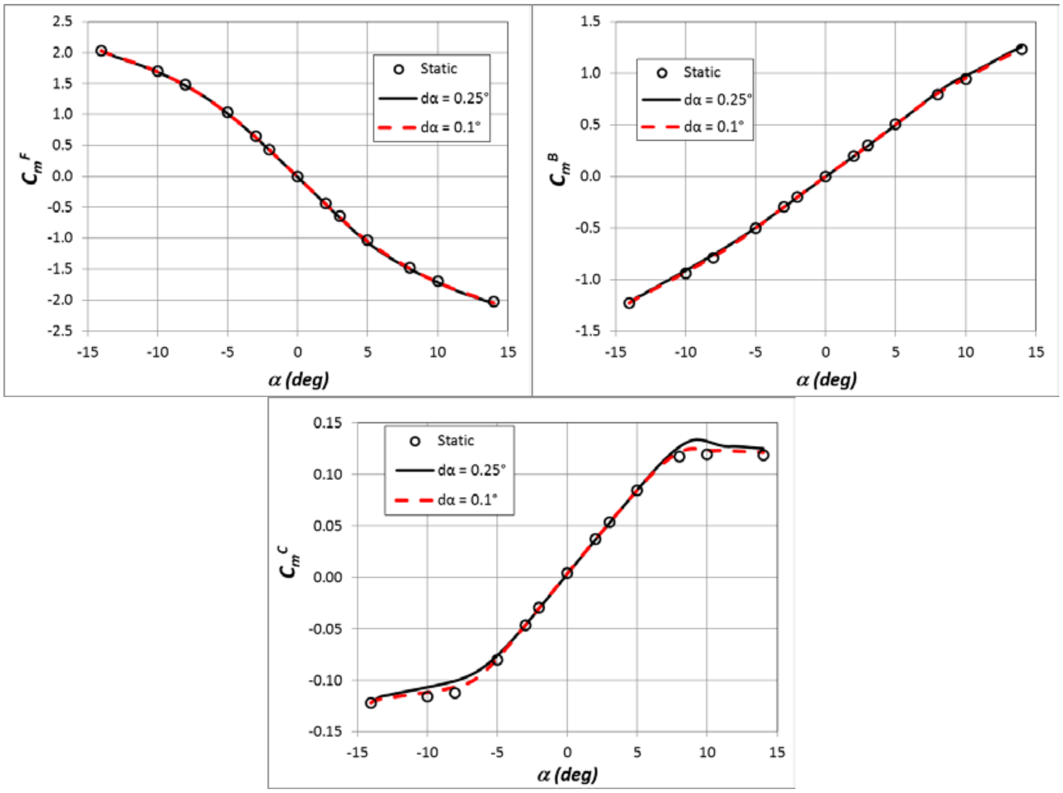

Fig. 21 Component contributions to pitching-moment coefficient for BFC0 with CFL = 10, N = 50, $d\alpha$ comparison

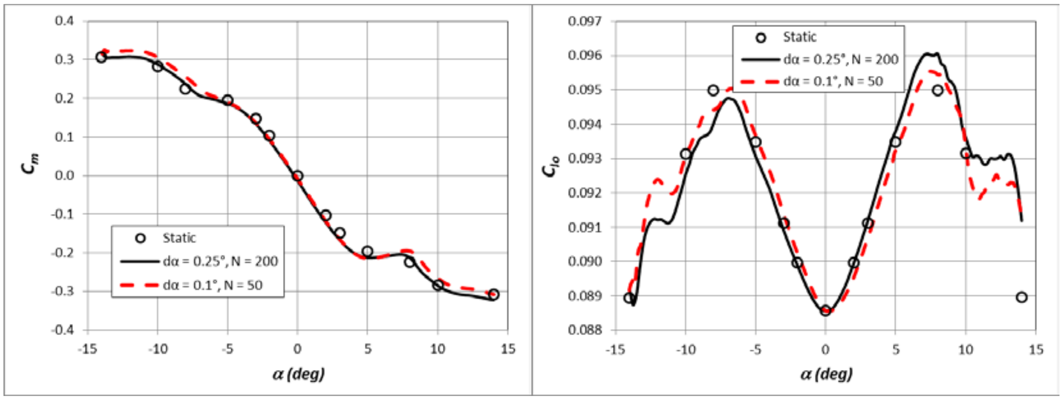

Fig. 22 Improved agreement for pitching-moment and roll-torque coefficients for BFC0 for CFL = 10, with N = 200 for larger $d\alpha$

While it is possible that a smaller $d\alpha$ or an increased number of inner iterations could lead to a more accurate sweep solution for the BFC0, the amount of computing time required to achieve the more accurate solutions would eliminate the efficiency of the quasi-steady sweep procedure. Thus, $d\alpha = 0.1°, N = 100$ was not investigated for improved agreement between the static and quasi-steady sweep results for C_m and C_{l_o}. Based on the results of the BF—using a larger CFL, similar to that used to converge the steady-state solutions, for the quasi-steady sweeps produced more reliable results—the remainder of the quasi-steady sweeps for the BFC0 were completed with CFL = 50.

As was the case for quasi-steady sweeps on the BF when CFL = 50, N = 100 was found to produce a converged solution for both $d\alpha$ investigated (0.25°, 0.1°), the size of $d\alpha$ did not matter with the larger CFL. The inner-iteration convergence histories were similar to those found for the BF (Fig. 9). For CFL = 50, N = 100, significantly better agreement was found between the static results and the quasi-steady sweep results for both C_m (Fig. 23) and C_{l_o} (Fig. 24) for the BFC0. Prediction of the body and fin component contributions to C_m by the sweep procedure remained good with the better-converged inner iterations as would be expected. Canard stall was now properly captured (when compared to the steady-state solutions) with proper inner-iteration convergence even for $d\alpha = 0.25°$ (Fig. 25). While it is possible an adequately converged sweep solution could still be obtained for $d\alpha = 0.5°$, it was decided that $d\alpha = 0.25°$ was sufficiently large enough due to the small discrepancies that were being observed in the BF.

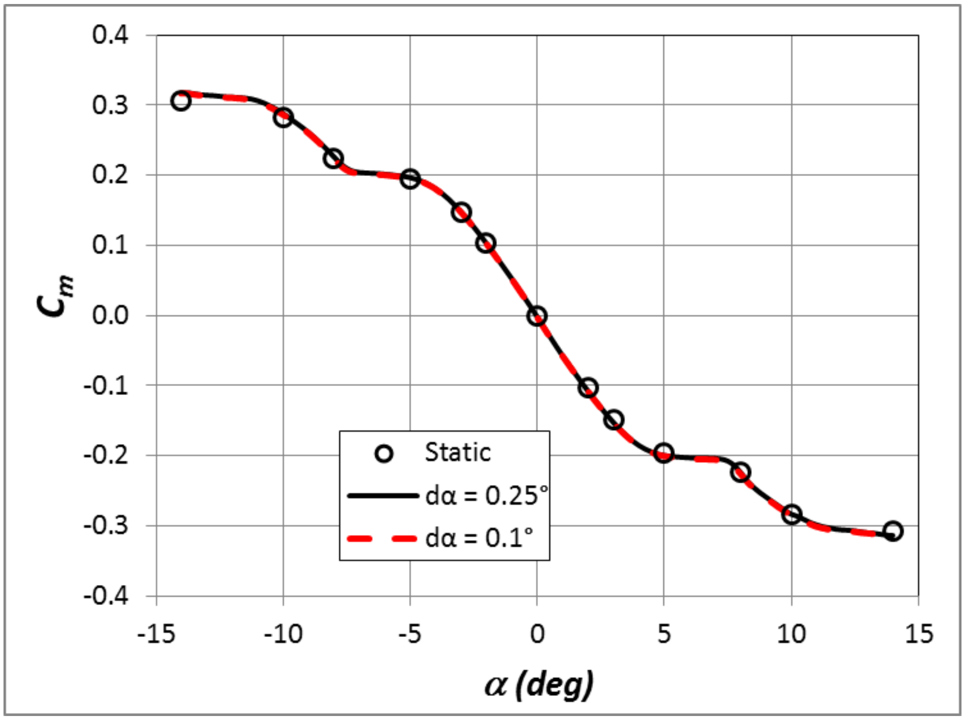

Fig. 23 Pitching-moment coefficient for BFC0 with CFL = 50, N = 100, $d\alpha$ comparison

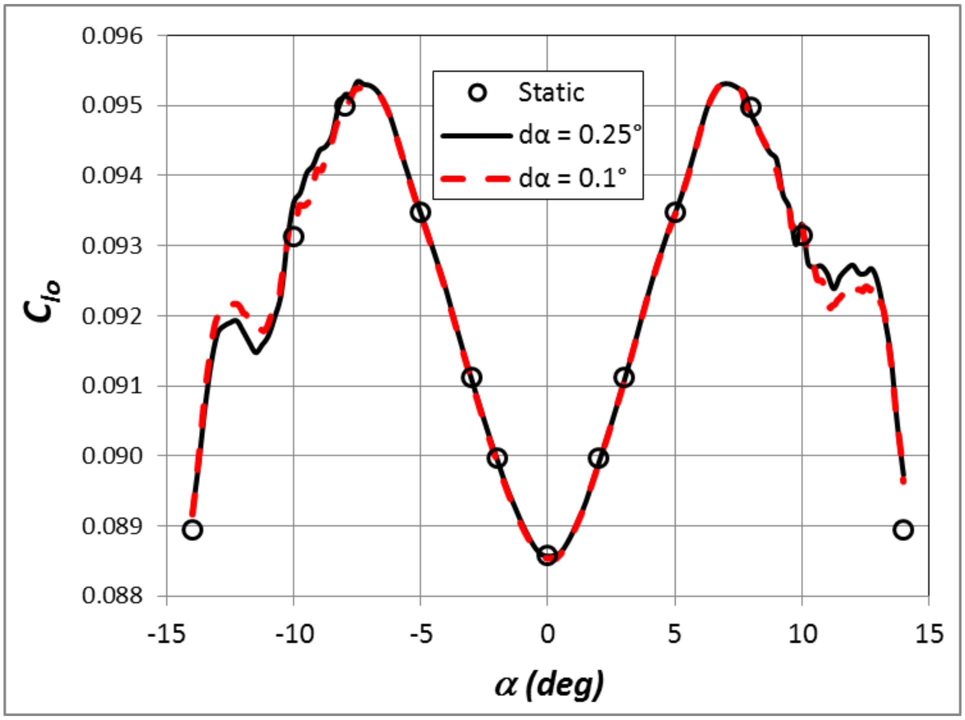

Fig. 24 Roll-torque coefficient for BFC0 with CFL = 50, N = 100, $d\alpha$ comparison

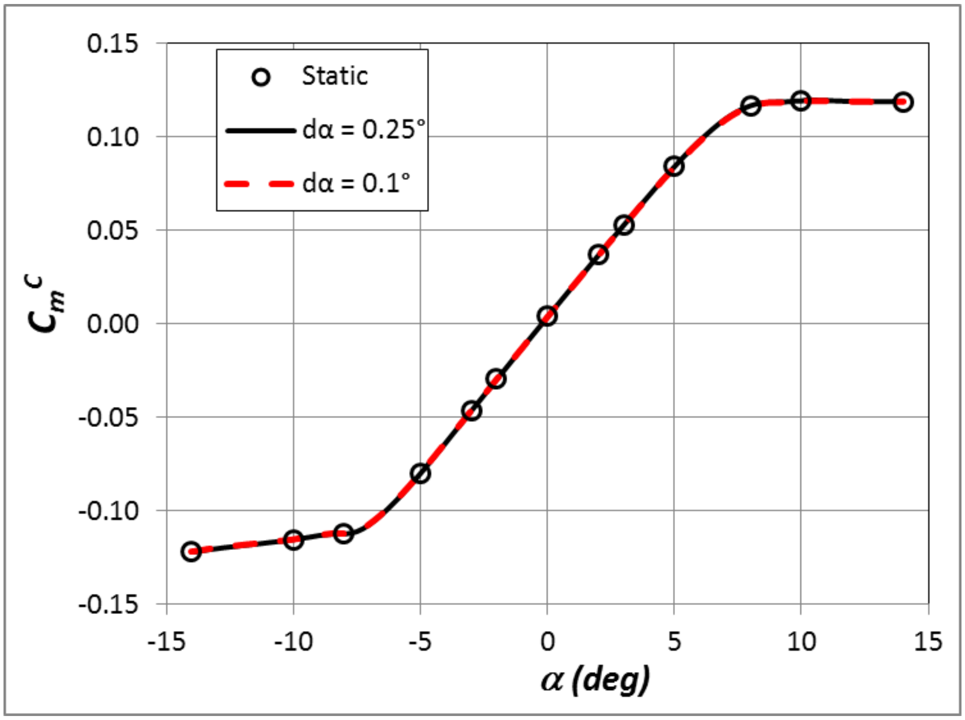

Fig. 25 Single canard component contribution to pitching-moment coefficient for BFC0 with CFL = 50, N = 100, $d\alpha$ comparison

The time savings achieved in obtaining the solutions for the BFC0 using the quasi-steady sweep procedure as compared to the steady-state method is even greater than it was for the BF. The BFC0 solutions were completed on 384 cores of the SGI ICE X supercomputer SPIRIT at the US Air Force Research Laboratory's Department of Defense Supercomputing Resource Center. A single steady-state solution could be obtained in approximately 5 h. That means, just to obtain the 13 steady-state solutions for comparison here took 65 wall-clock h or 24,960 CPU h. The sweep procedure using $d\alpha = 0.25°$ (CFL = 50, N = 100) took just 37.7 wall-clock h (14,477 CPU h), a 42% time savings. This would significantly improve resolution for predicting stall while greatly reducing resources. Increasing resolution further by using $d\alpha = 0.1°$ (CFL = 50, N = 100) increases use of computing resources to 37,900 CPU h. While this is 50% increase in use of resources over that used to generate the steady-state solutions presented here, a lot more data were generated with those resources.

4.2.2 δ = 4°

The final case considered as part of this study was the body–fin–canard configuration with the canards deflected to 4° for pitch control (BFC4). A deflected-canard configuration was investigated to ensure the variations in the flow that occur when the canards are deflected (separation, stall, vortex shedding, vortex–fin interaction, etc.) did not cause a change in sweep's critical parameters.

Convergence criteria for CFL = 10 were again investigated because it was thought that a more complicated configuration (i.e., more flow nonlinearities) may require a smaller CFL for convergence of the steady-state solution at high α, which would in turn limit the CFL for the sweep procedure. Due to the simpler BF requiring N = 200 for convergence of the quasi-steady sweep when $d\alpha = 0.25°$, only $d\alpha = 0.25°$ with N = 200 is compared to the results for $d\alpha = 0.1°$ and $d\alpha = 0.05°$ each with N = 50, which was the required number of inner iterations for convergence on the BF.

As with the previous configurations considered, only C_m and C_{l_o} showed any noticeable variation with $d\alpha$; the forces converge more quickly than the moments. The variation in C_m was only noticeable at $|\alpha| \geq 10°$ and even there it was typically less than 5% (Fig. 26). The variation in C_{l_o} was only noticeable for $|\alpha| \geq 8°$ and on an enlarged scale (Fig. 27). This further validates that it is not the $d\alpha$ that matters but, rather, that a sufficient number of inner iterations are completed such that convergence is reached (Fig. 27) for the chosen CFL number. A smaller $d\alpha$ requires fewer inner iterations and shows less inner-iteration residual drop as there are fewer changes in the flow between steps. This implies that if there are regions of α where the flow is more difficult to converge—thus requiring a smaller CFL number—the quasi-steady-sweep procedure can be completed with an increased number of inner iterations in the region; a smaller $d\alpha$ may not be required. This would, of course, require additional CPU time for the increased inner iterations.

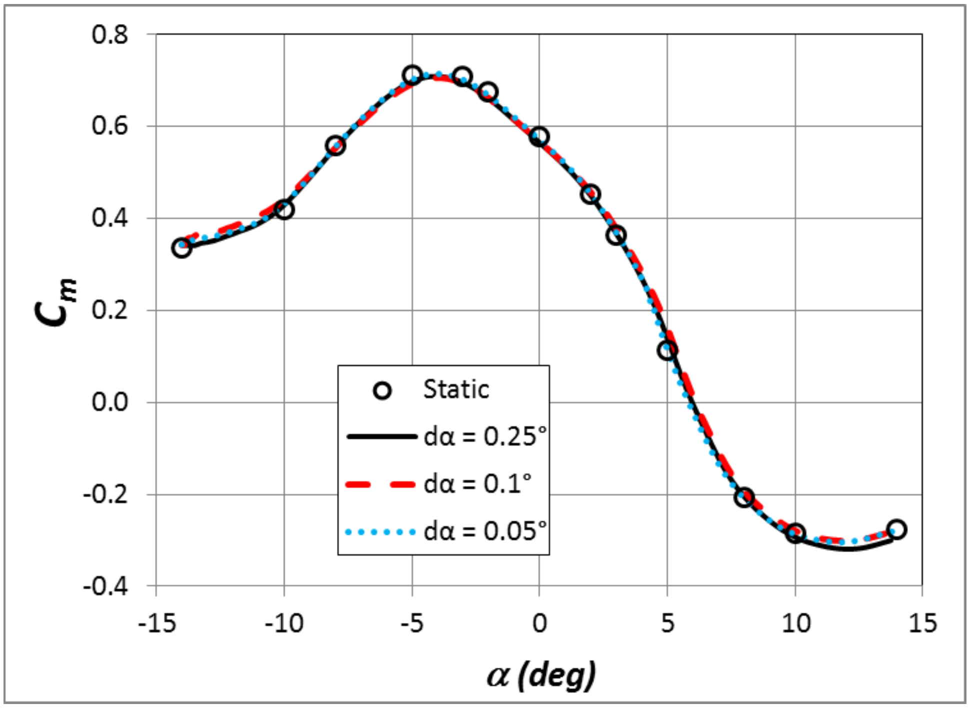

Fig. 26 ***C_m* comparison of BFC4 for CFL = 10 and *dα* = 0.25° with N = 200 to *dα* = 0.1° and *dα* = 0.05° with N = 50**

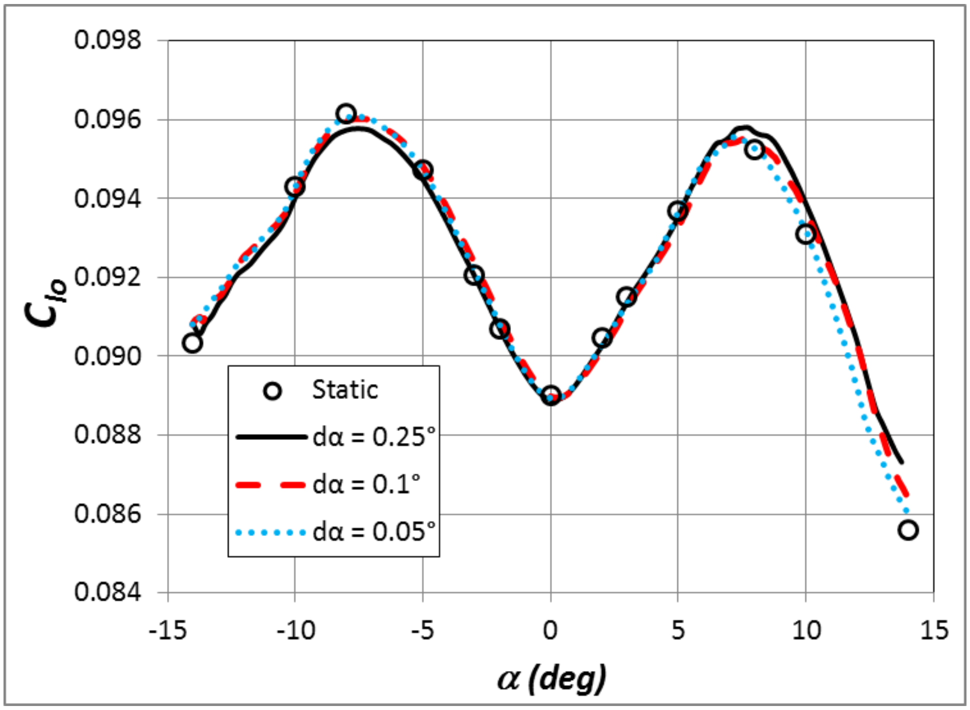

Fig. 27 ***C_{lo}* comparison of BFC4 for CFL = 10 and *dα* = 0.25° with N = 200 to *dα* = 0.1° and *dα* = 0.05° with N = 50**

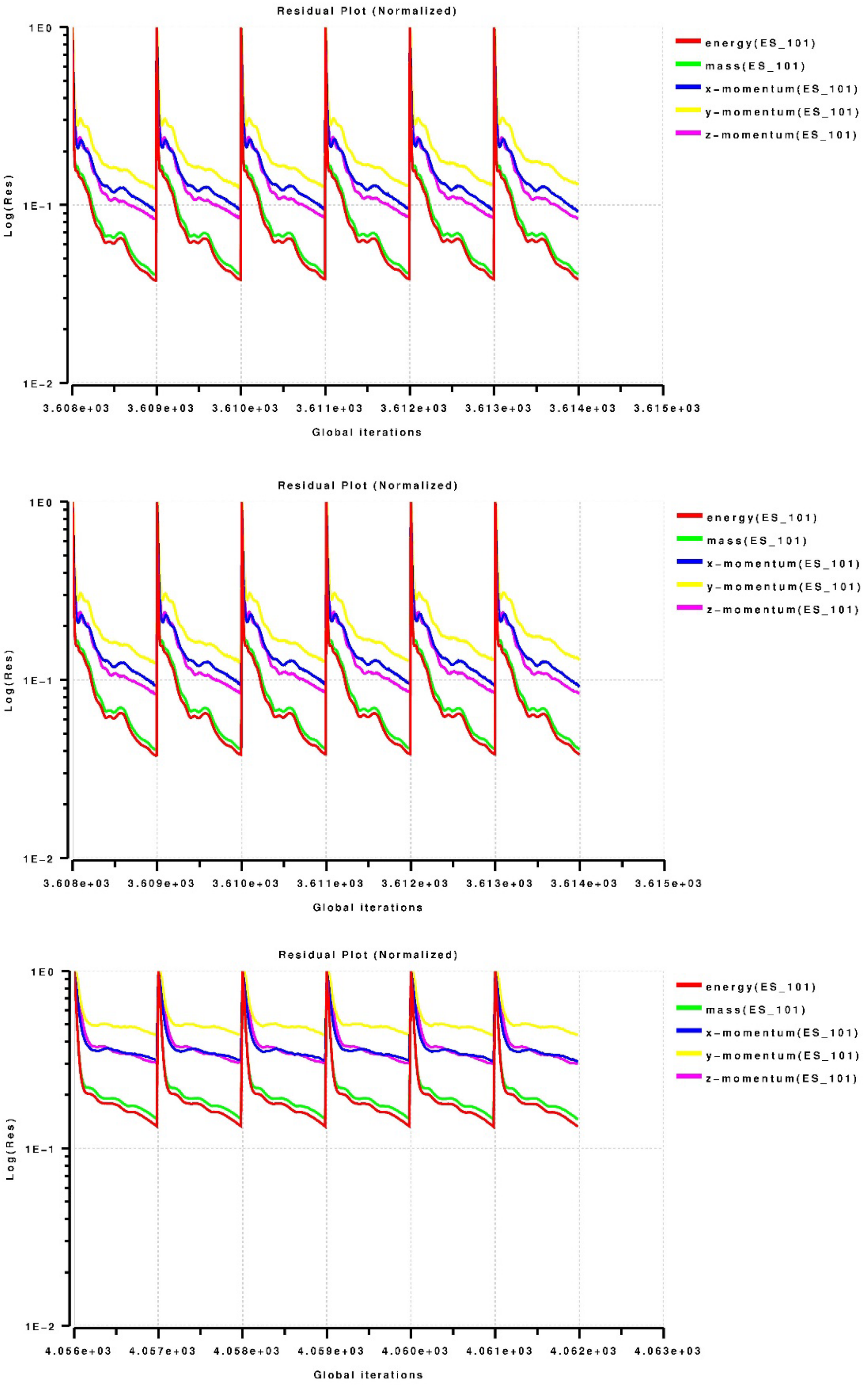

Fig. 28 Inner-iteration convergence history for BFC4 for CFL = 10, $d\alpha$ = 0.25° with N = 200 (top), $d\alpha$ = 0.1° with N = 50 (middle), and $d\alpha$ = 0.05° with N = 50 (middle)

Since CFL = 50, N = 100 produced better results at larger $d\alpha$ than a CFL = 10 for the BFC0, it was investigated for the BFC4 to determine if the quasi-steady sweep could be obtained any more efficiently. For CFL = 50, convergence of the inner-iteration residuals was confirmed for N = 100. Residual drops of approximately 2E-2 and 4E-2 were achieved for $d\alpha = 0.25°$ and $d\alpha = 0.1°$, respectively (Fig. 29). The residual drop is not as large for $d\alpha = 0.1°$ because there is less change in the flow due to the smaller change in α. For both increments, the residuals appear to be reaching a plateau, which indicates convergence. Therefore, N = 100 was used and no further inner-iteration convergence was investigated for CFL = 50.

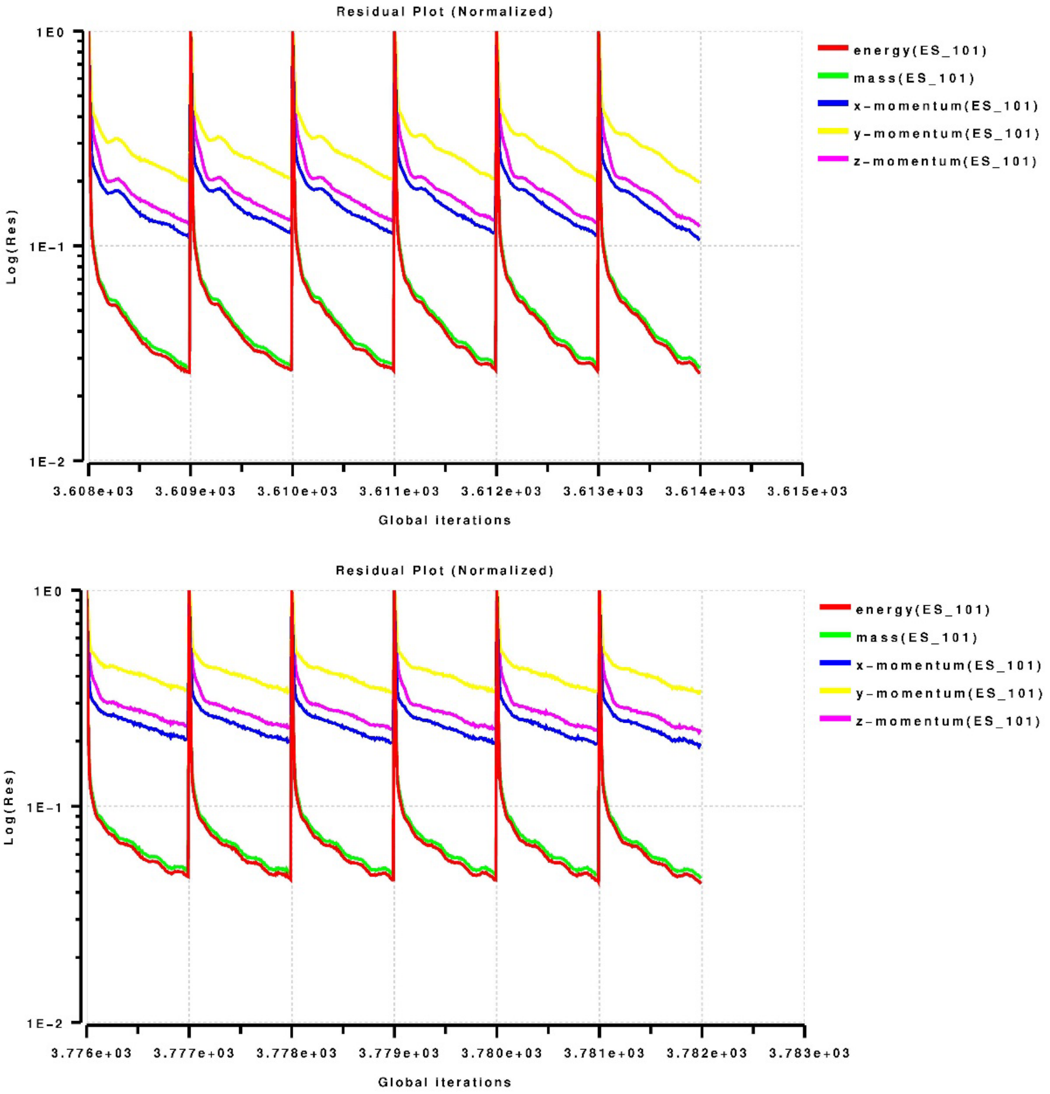

Fig. 29 Inner-iteration convergence history for BFC4 with CFL = 50, N = 100; $d\alpha$ = 0.25° (top) and $d\alpha$ = 0.1° (bottom)

The true test of inner-iteration convergence is the comparison of the quasi-steady-sweep procedure's results to the results obtained from the steady-state methodology. All force and moment coefficients (Figs. 30–33) show very good agreement with the solutions from the steady-state methodology, indicating the inner iterations must indeed be converged. Even the nonlinearity in the moment coefficients is accurately captured. From the analysis of C_m^C for each canard (Fig. 34), canard-stall angle is known to within a 0.25°; no interpolation is necessary.

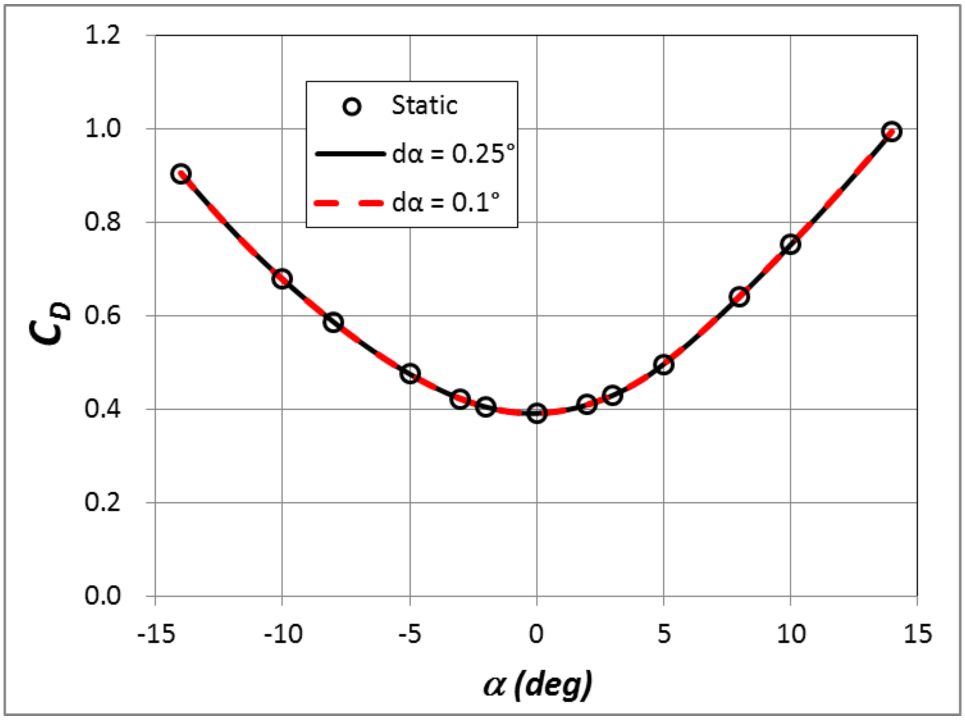

Fig. 30 Drag coefficient for BFC4 with CFL = 50, N = 100, $d\alpha$ comparison

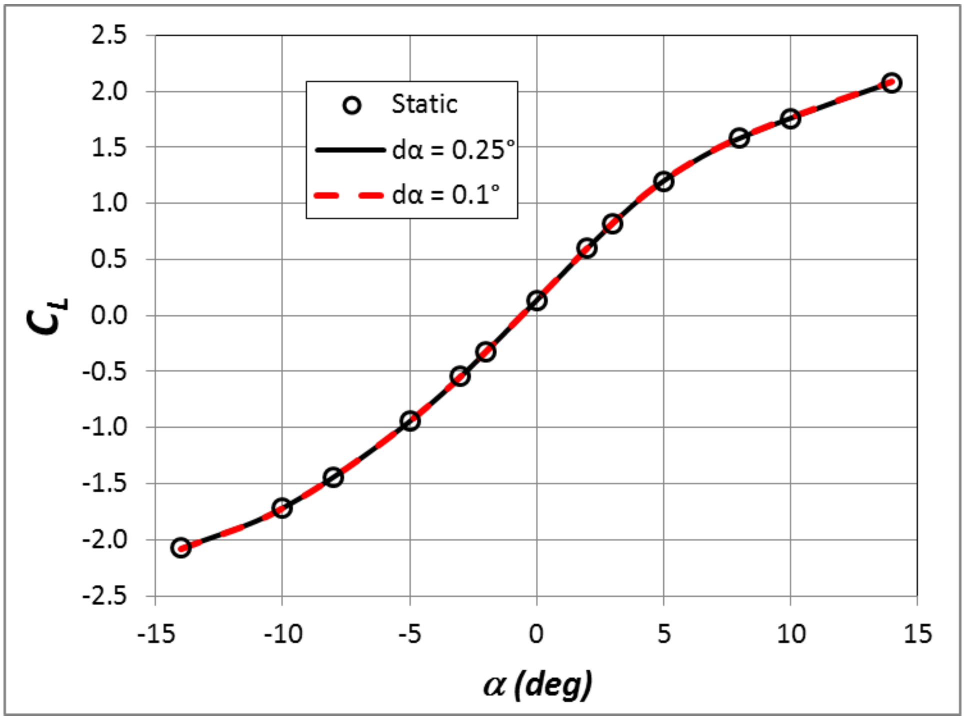

Fig. 31 **Lift coefficient for BFC4 with CFL = 50, N = 100, $d\alpha$ comparison**

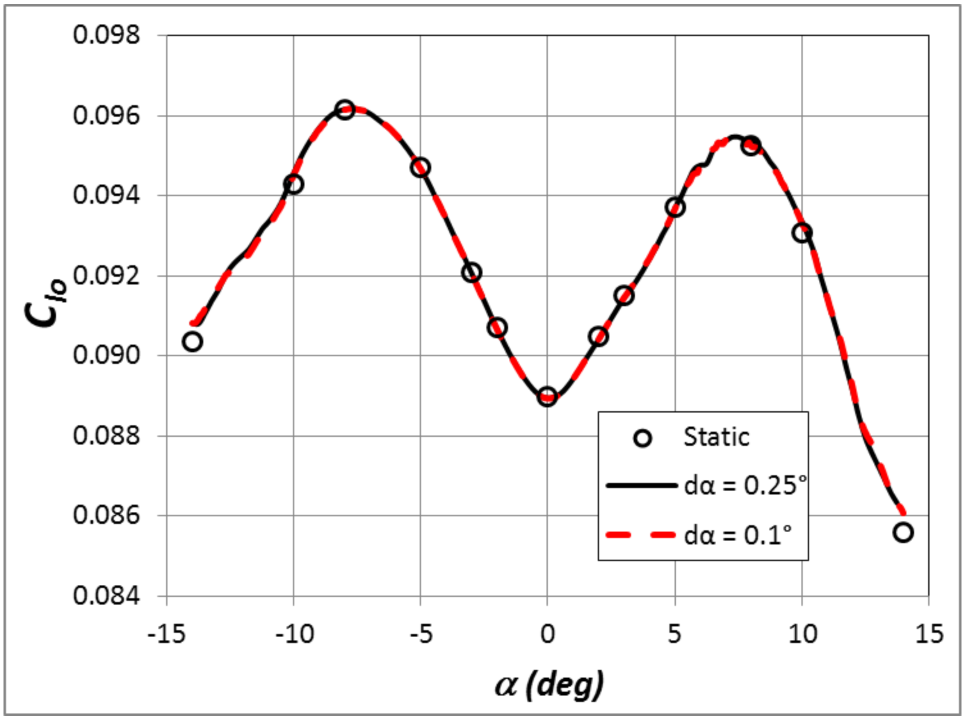

Fig. 32 **Roll-torque coefficient for BFC4 with CFL = 50, N=100, $d\alpha$ comparison**

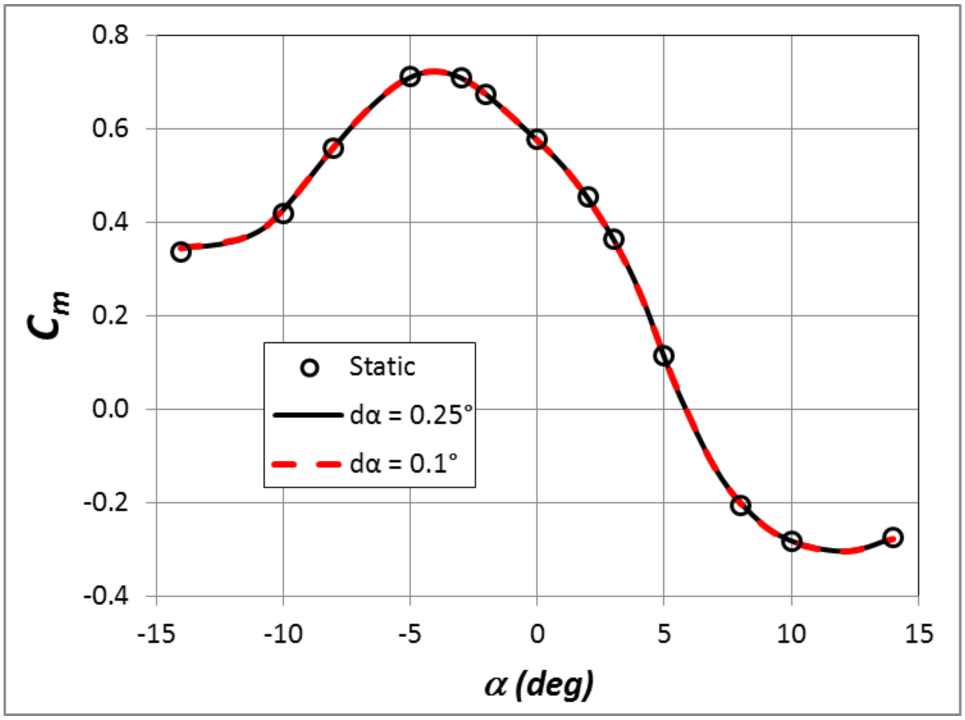

Fig. 33 Pitching-moment coefficient for BFC4 with CFL = 50, N = 100, $d\alpha$ comparison

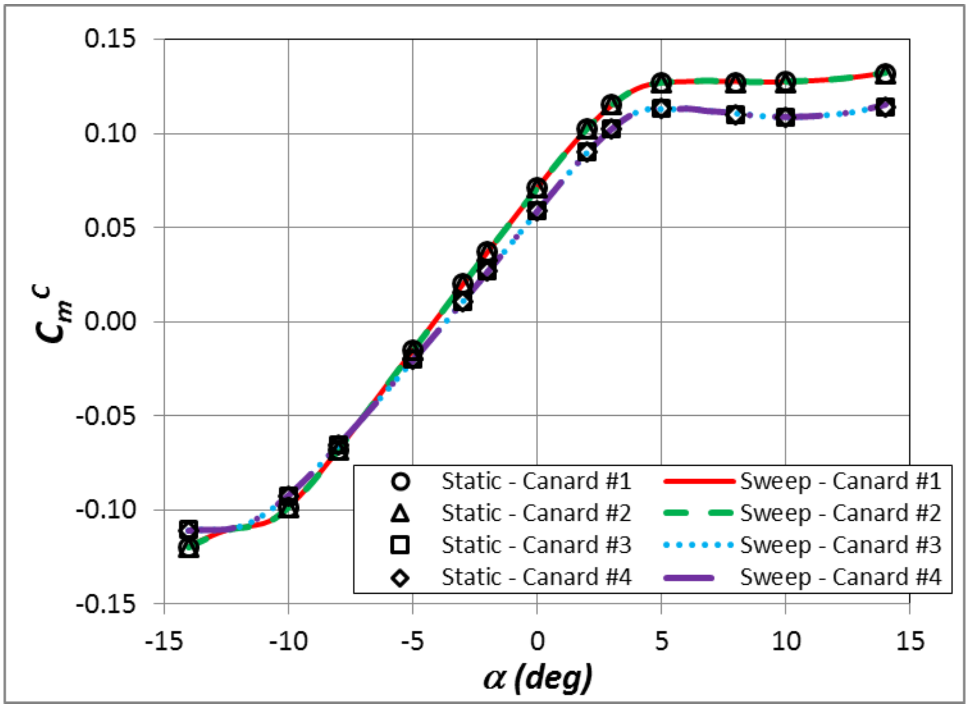

Fig. 34. Individual canards' pitching-moment contributions with $d\alpha$ = 0.25°, CFL = 50, N = 100

As the mesh size for the BFC4 is approximately the same as that of the BFC0, the required computational time was found to be similar. For $d\alpha = 0.25°$, 36.5 wall-clock h on 384 cores of the SGI ICE X cluster (approximately 14,000 CPU h) were required. For $d\alpha = 0.1°$, 86.3 wall-clock h on 384 cores of the SGI ICE X cluster (approximately 33,000 CPU h) were necessary. Compare this to a required wall-clock time of 3.8 h (1,460 CPU h) for the steady-state solution. The break-even point is 10 steady-state solutions. If more than 10 steady-state solutions are required to adequately resolve the static coefficients, which is likely the case of a highly nonlinear flow such as this, the sweep procedure is definitely the more efficient method. The increment is dependent on the resolution desired as was the case with the BFC0. The physics is being adequately captured.

5. Conclusions

A quasi-steady sweep procedure that allows determination of the static aerodynamic coefficients for a range of angles of attack in a single simulation is extended to subsonic Mach numbers. Given a steady-state solution, the procedure can be used to generate multiple quasi-steady numerical simulations over a select range of angles of attack for a given set of flight conditions. Computational fluid-dynamics simulations are completed for the ARL-designed HMA, a canard-controlled, fin-stabilized projectile, at Mach 0.65 for a moderate range of angles of attack ($-14° \leq \alpha \leq 14°$) using the sweep procedure. Separate steady-state solutions were also computed at various angles of attack within this range for comparison.

Three configurations of the HMA geometry were considered to evaluate the sweep procedure for increasingly complex geometries: 1) body–fin, 2) body–fin–canard at 0° canard-deflection angle, and 3) body–fin–canard with canards deflected 4° for a pitch up maneuver. For each configuration, the parameters of $d\alpha$, CFL number, and number of inner iterations were varied to find the most efficient combination to achieve a converged solution. The initial values used for these parameters, based on previous findings for supersonic velocities, were found to be insufficient in the subsonic regime to find agreement with the steady-state solution for C_m and C_{l_o}.

Inner-iteration convergence is critical to accurate solutions for the quasi-steady sweep procedure. Depending on the CFL number and $d\alpha$ chosen, inner-iteration convergence is achieved when a magnitude drop of greater than 1E-2 in residuals occurs or the residual levels do not vary significantly; the inner-iteration convergence needs to be checked periodically during the sweep to ensure there is not an angle of attack that is having difficulty converging. If inner iterations are having difficulty converging during just a section of the sweep trajectory, the CFL number could be reduced and either the $d\alpha$ could be reduced or the number of inner iterations increased (or both) for that section to ensure convergence throughout the range of angles of attack.

Variation of CFL number in the sweep procedure showed that agreement with the steady-state solution could be approached for either CFL = 10 or CFL = 50 for any of the 3 configurations if a sufficient number of inner iterations and a sufficiently small $d\alpha$ were used. Using CFL = 50, $d\alpha = 0.25°$, and N = 100, the sweep procedure was found to achieve excellent agreement with the aerodynamic forces and moments obtained from the steady-state method for all 3 configurations. The CFL = 10 required the use of a smaller $d\alpha$ (0.1° versus 0.25°) and/or an increased number of inner iterations (200 versus 100) to achieve convergence as compared to CFL = 50 to obtain results that were in reasonable agreement with the C_m and C_{l_o} values obtained from the steady-state method. Thus, convergence occurs more quickly when a larger CFL number is used, as would be expected. However, if the CFL number needs to be limited to achieve a converged flow field, inner-iteration convergence can still be achieved with use of smaller $d\alpha$ or an increased number of inner iterations.

Although smaller dα values and more inner iterations are required to obtain accurate moment coefficients from the sweep procedure for a subsonic flow, the quasi-steady sweep procedure remains an efficient means of obtaining a range of angles of attack for a given set of flow conditions. A typical steady-state solution at one angle of attack for the BFC4 took 1,460 CPU h (approximately 3.5 h on 384 cores). The sweep procedure with CFL = 50, $d\alpha = 0.25°$, N = 100 required approximately 14,000 CPU h (approximately 36.5 h on 384 cores). This means that in the time it would take to complete 10 steady-state solutions, a solution with 112 angles was generated. For a complex configuration that may potentially have nonlinear forces and moments, this increased resolution is critical. For a less complex configuration such as the BF, where the forces and moments are known to be linear, the increased resolution of the sweep procedure is not necessary; greater efficiency could be achieved by just choosing a small number of angles of attack to simulate with the steady-state method and using standard curve fit procedures to generate data at the other angles.

6. References

Arrow Tech Associates. PRODAS V3 user manual Burlington (VT); 2015.

Bhagwandin VA. Numerical prediction of roll damping and magnus dynamic derivatives for finned projectiles at angle of attack. Paper presented at: 30th AIAA Applied Aerodynamics Conference; 2012 Jun 25–28; New Orleans (LA). Paper No.: AIAA-2012-2905.

Bhagwandin VA. Numerical prediction of shock-boundary layer interaction between a pair of fins in hypersonic flow. Paper presented at: 44th AIAA Fluid Dynamics Conference; 2014 Jun 16–20; Atlanta (GA). Paper No.: AIAA-2014-3337.

Bhagwandin VA. Numerical prediction of planar shock wave interaction with a cylindrical body. Paper presented at: 53rd AIAA Aerospace Sciences Meeting; 2015 Jan 5–9; Kissimmee (FL). Paper No.: AIAA-2015-1940.

Bhagwandin VA, Sahu J. Numerical prediction of pitch damping stability derivatives for finned projectiles. J Space Roc. 2014;51(5):1603–1618.

Camargo J, Lopez O, Ochoa-Lleras N. A computational tool for unsteady aerodynamic flow simulations coupled with rigid body dynamics and control. Paper presented at: 30th AIAA Applied Aerodynamics Conference; 2012 Jun 25–28; New Orleans (LA). Paper No.: AIAA-2012-3034.

Costello M, Gatto S, Sahu J. Using CFD/RBD results to generate aerodynamic models for projectile flight simulation. Paper presented at: AIAA Atmospheric Flight Mechanics Conference and Exhibit; 2007 Aug 20–23; Hilton Head (SC). Paper No.: AIAA-2007-6582.

Coyle CJ, Silton SI. CFD aerodynamic characterization of a high maneuverability airframe. Paper presented at: 33rd AIAA Applied Aerodynamics Conference; 2015 Jun 22–26; Dallas (TX). Paper No.: AIAA-2015-3015.

Dassault Systemes SolidWorks Corporation. SolidWorks 2012; Waltham (MA).

Da Ronch A, Vellespin D, Ghoreyshi M, Badcock KJ. Evaluation of dynamic derivatives using computational fluid dynamics. AIAA Journal. 2012;50(2):470–484.

DeBonis JR, Oberkampf WL, Wolf RT, Orkwis PD, Turner MG, Babinsky H, Benek JA. Assessment of computational fluid dynamics and experimental data for shock boundary-layer interactions. AIAA Journal. 2012;50(4):891–903.

DeSpirito J. CFD prediction of magnus effect in subsonic to supersonic flight. Paper presented at: 46th AIAA Aerospace Sciences Meeting and Exhibit; 2008 Jan 7–10; Reno (NV). Paper No.: AIAA-2008-427.

DeSpirito J, Heavey KR. CFD computations of magnus moment and roll-damping moment of a spinning projectile. Paper presented at: AIAA Atmospheric Flight Mechanics Conference and Exhibit; 2004 Aug 16–19; Providence (RI). Paper No.: AIAA-2004-4713.

DeSpirito J, Plostins P. CFD prediction of M910 projectile aerodynamics: unsteady wake effect on magnus moment. Paper presented at: AIAA Atmospheric Flight Mechanics Conference and Exhibit; 2007 Aug 20–23; Hilton Head (SC). Paper No.: AIAA-2007-6580.

DeSpirito J, Silton SI, Weinacht P. Navier-stokes predictions of dynamic stability derivatives: evaluation of steady-state methods. J Space Roc. 2009;46(6):1142–1154.

DeSpirito J, Vaughn, M, Washington. Numerical investigation of canard-controlled missile with planar grid fins. J Space Roc. 2003;40(3):363–370.

Fresconi F, Celmins I, Fairfax L. Optimal parameters for maneuverability of affordable precision munitions. Aberdeen Proving Ground (MD): Army Research Laboratory (US); 2011 Aug. Report No.: ARL-TR-5647.

Fresconi F, Celmins I, Silton SI. Theory, Guidance and flight control for high maneuverability projectiles. Aberdeen Proving Ground (MD): Army Research Laboratory (US); 2014 Jan. Report No.: ARL-TR-6767.

Goldberg U, Peroomian O, Chakravarthy S. A wall-distance-free k-ε model with enhanced near-wall treatment. J Fluids Eng. 1998;120(3):457–462.

Klatt D, Hruschka R, Leopold F. Numerical and experimental investigation of the magnus effect in supersonic flows. Paper presented at: 30th AIAA Applied Aerodynamics Conference; 2012 Jun 25–28; New Orleans (LA). Paper No.: AIAA-2012-3230.

Lesieutre DJ, Love JF, Dillenius MFE. Recent applications and improvements to the engineering-level aerodynamic prediction software MISL3. Paper presented at: 40th AIAA Aerospace Sciences Meeting and Exhibit; 2002 Jan 14–17; Reno (NV). Paper No.: AIAA-2002-0275.

Metacomp Technologies, Inc. MIME user manual. Agoura Hills (CA); 2010.

Metacomp Technologies, Inc. CFD++ user manual. Agoura Hills (CA); 2011.

Moore FG, Moore LY. 2009 version of the aeroprediction code: AP09. J Space Roc. 2008;45(4):677–690.

Montalvo C, Costello M. Estimation of projectile aerodynamic coefficients using coupled CFD/RBD simulation results. Paper presented at: AIAA Atmospheric Flight Mechanics Conference; 2010 Aug 2–5; Toronto, Ontario, Canada. Paper No.: AIAA-2010-8249.

Murman SM. Reduced-frequency approach for calculating dynamic derivatives. AIAA Journal. 2007;45(6):1161–1168.

Oktay E, Akay H. CFD predictions of dynamic derivatives for missiles. Paper presented at: 40th AIAA Aerospace Sciences Meeting and Exhibit; 2002 Jan 14–17; Reno (NV). Paper No.: AIAA 2002-0276.

Park SH, Kwon JH. Comparisons of steady and unsteady methods for pitch-damping predictions. Paper presented at: 21st AIAA Applied Aerodynamics Conference; 2003 Jun 23–26; Orlando (FL). Paper No.: AIAA-2003-3671.

Rosema C, Doyle J, Auman L, Underwood M, Blake WB. Missile DATCOM user's manual–2011 revision. Wright–Patterson AFB (OH): Air Force Research Laboratory (US); 2011 Mar. Report No.: AFRL-RB-WP-TR-2011-3071.

Sahu J. Numerical computations of transonic critical aerodynamic behavior. AIAA Journal. 1990;28(5):807–816.

Sahu J. Coupled CFD and rigid body dynamics modeling of a spinning body with flow control. Paper presented at: 2nd AIAA Flow Control Conference; 2004 Jun 28–Jul 1; Portland (OR). Paper No.: AIAA-2004-2317.

Sahu J. Time-accurate numerical prediction of free-flight aerodynamics of a finned projectile. J Space Roc. 2008;45(5):946–954.

Sahu J. Computations of unsteady aerodynamics of a spinning body at transonic speeds. Paper presented at: 27th AIAA Applied Aerodynamics Conference; 2009 Jun 22–25; San Antonio (TX). Paper No.: AIAA-2009-3852.

Sahu J. Unsteady aerodynamic simulations of a canard-controlled projectile at low transonic speeds. Paper presented at: AIAA Atmospheric Flight Mechanics Conference; 2011 Aug 8–11; Portland (OR). Paper No.: AIAA-2011-6336.

Sahu J, Fresconi F. Aeromechanics of control of projectile roll using coupled simulation techniques. J Space Roc. 2015;52(3):944–957.

Sahu J, Heavey KR. Time-accurate computations for rapid generation of missile aerodynamics. Paper presented at: Atmospheric Flight Mechanics Conference; 2010 Aug 2–5; Toronto, Ontario, Canada. Paper No.: AIAA-2010-8248.

Scheuermann E, Costello M, Silton S, Sahu, J. Aerodynamic characterization of a microspoiler system for supersonic finned projectiles. J Space Roc. 2015;52(1):253–263.

Silton S. Navier-stokes computations for a spinning projectile from subsonic to supersonic speeds. J Space Roc. 2005;42(2):223–231.

Silton SI. Navier-stokes predictions of aerodynamic coefficients and dynamic derivatives of a 0.50-cal projectile. Paper presented at: 29th AIAA Applied Aerodynamics Conference; 2011 Jun 27–30; Honolulu (HI). Paper No.: AIAA-2011-3030.

Silton SI, Fresconi FE. High maneuverability airframe: initial investigation of configuration aft end for increased stability, range, and maneuverability. Aberdeen Proving Ground (MD): Army Research Laboratory (US); 2013 Sep. Report No.: ARL-TR-6585.

Silton SI, Coyle CJ. Effect of canard deflection on fin performance of a fin-stabilized projectile. Paper presented at: 33rd AIAA Applied Aerodynamics Conference; 2015 Jun 22–26; Dallas (TX). Paper No.: 2015-2586.

Silton SI, Fresconi FE. Effect of canard interactions on aerodynamic performance of a fin-stabilized projectile. J Space Roc; 2015;52(5):1430–1442.

Silton SI, Fresconi F, Celmins I. High maneuverability airframe: investigation of fin and canard sizing for optimum maneuverability. Aberdeen Proving Ground (MD): Army Research Laboratory (US); 2014 Sep. Report No.: ARL-TR-7052.

Stahl J, Costello M, Sahu J. Projectile aerodynamic coefficient estimation using integrated CFD/RBD and flight control system modeling. Paper presented at: AIAA Atmospheric Flight Mechanics Conference; 2009 Aug 10–13; Chicago (IL). Paper No.: AIAA-2009-5715.

Wang G, Zheng Z, Suo Q. Trajectory simulation of a spinning projectile based on variable step size CFD/RBD method. Paper presented at: AIAA Atmospheric Flight Mechanics Conference; 2015 Jan 5–9; Kissimmee (FL). Paper No.: AIAA-2015-0522.

Weinacht P, Sturek WB. Navier-stokes predictions of pitch damping for finned projectiles using steady coning motion. Paper presented at: Flight Simulation Technologies Conference and Exhibit; 1990 Sep 17–19; Dayton (OH). Paper No.: AIAA-1990-3088.

Appendix. Quasi-Steady Sweep's Implementation in CFD^{++}

The CFD^{++} implementation of the sweep procedure is fairly typical of any computational fluid dynamics solver. There are, however, a number of nuances in this particular solver that the author believed should be documented. All have to do with the setup of the procedure and not the actual solution.

In initializing the quasi-steady sweep procedure (and all time-accurate simulations) in CFD^{++}, one must first determine how they want to start: reset the step to zero or continue from the last step in the steady-state solution; the time always starts from a value of 0. If one chooses to continue from the last step in the steady-state solution, the following does not affect the solution; but, if one chooses to reset the step to zero—the author's preference for the sweep procedure—the following must be completed. There are a number of equations that are not turned on at Step 0 by default. These include preconditioning and turbulence modeling. These can be easily set to start at Step 0 either in the steady to unsteady wizard or in the Reimann Solver and Turbulence Control panels, respectively. The author recently found the additional transport equations are solved in nonconservation mode for the first 20 steps in CFD^{++} by default. Prior to Version 15.1 Update 4, one had to add the option "iftcon_ntstart 0" to the mcfd.inp input file such that the additional transport equations are solved in conservation mode from Step 0. In Version 15.1 Update 4 and later, there is an "Extra Eqns" button in the second panel of the Time Integration Panel. By choosing this "Extra Eqns" Panel, one can change the conservation updates for the equations for turbulence, scalars, and species to start at Step 0. This ensures that every single step is physically relevant. Although not relevant to this subsonic simulation, one also needs to ensure that 1st- to 2nd-order spatial discretization blending is turned off and that the Right Hand Side dissipation is 0 for the time-accurate solution that starts at Step 0 if either was used to obtain the steady-state simulation.

CFD^{++} uses file-based rotation to complete the mesh motion used for the sweep procedure. For the case considered here, only single-axis rotational motion in the body frame is required. As per the CFD^{++} help, the file format is as follows:

Origin (x y z values)

Direction vector (x y z values)

datalines

Time1 (s) rotation_angle1 (radians) rotation_rate1 (radians/s)

Time2 (s) rotation_angle2 (radians) rotation_rate2 (radians/s)

For an angle-of-attack sweep, the origin should be at the center of gravity. If the origin of the computational domain is at the center of gravity, this is (0, 0, 0). If the origin of the computational domain is at another location, the center of gravity's location relative to the origin of the computational domain should be entered.

The directional vector is self-explanatory. For an alpha sweep, with the x-axis aligned with (and pointing downstream) the flow and the z-axis up, the rotational axis is the y-axis. Therefore the directional vector would be (0 1 0).

For an angle-of-attack sweep where a single angle-of-attack increment ($d\alpha$) is utilized, only 2 data lines are required. Because the sweep procedure always starts from time zero, regardless of whether or not you reset the step to zero, the first data line is at time zero with a rotation angle of zero. The rotation angle is zero because the steady-state solution from which the quasi-steady sweep is initialized is obtained on the computational domain that has been rotated to the minimum angle of attack desired. The second data line is a bit more complicated. The final time ($Time_{final}$) is the total angle of sweep (α_{sweep}) divided by the increment (Eq. A-1). The rotation angle is the total angle of sweep in radians, which for $-14^\circ \leq \alpha \leq 14^\circ$ is 28° or 0.4886922 radians. CFD^{++} calculates the time-accurate solution at the starting angle of attack on Step 1; the mesh is not rotated until the end of Step 1. Therefore, to obtain the full range of the sweep it is necessary to calculate a solution for one additional increment. This means a total of 113 (including 0) seconds (steps) are simulated.

$$Time_{final} = \frac{\alpha_{sweep}}{d\alpha} \tag{A-1}$$

The contents of the file for the alpha sweep performed here is shown below:

```
0      0      0
0      1      0
2
0      0.0000000      0
112    0.4886922      0
```

If more than one $d\alpha$ needs to be utilized to ensure resolution, an additional data line can be added for each additional increment desired. The first data line remains the same as in the previous case as the mesh is at $\alpha = -14^\circ$ to start the simulations. Equation A-2 is now used for each additional data line.

$$Time_i = \frac{\alpha_{sweep_i}}{d\alpha_i} + Time_{i-1} \quad , \tag{A-2}$$

where

$$\alpha_{sweep_i} = \alpha_{i_{final}} - \alpha_{i_{initial}} \quad : \tag{A-3}$$

$\alpha_{i_{final}}$ is the final angle in the increment and $\alpha_{i_{initial}}$ is the initial angle on the increment. The value for the second column is determined by

$$\text{rotation\_angle}_i = \alpha_{i_{final}} - \alpha_{initial} \tag{A-4}$$

where α_{intial} is the initial angle of attack. For example, if it was desired to use $d\alpha = 0.1$ for $-14° \leq \alpha \leq -9°$, $d\alpha = 0.25$ for $-9° \leq \alpha \leq 3°$, and $d\alpha = 0.1$ for $3° \leq \alpha \leq 14°$, the content of the file for the alpha-sweep procedure would be as shown below and a total of 209 s (i.e., steps) simulated.

```
0     0     0
0     1     0
4
0     0.0000000     0
50    0.0872665     0
98    0.2967060     0
208   0.4886922     0
```

List of Symbols, Abbreviations, and Acronyms

3-D	3-dimensional
ARL	US Army Research Laboratory
BF	body–fin configuration
BFC0	body–fin–canard configuration with $\delta = 0°$
BFC4	body–fin–canard configuration with $\delta = 4°$
C_D	drag coefficient
C_L	lift coefficient
C_{l_o}	roll-torque coefficient
C_m	pitching-moment coefficient
$d\alpha$	angle-of-attack increment
CFD	Computational Fluid Dynamics
CFL	Courant–Friedrichs–Lewy number
CPU	central processing unit
HMA	high-maneuverability airframe
M	Mach number
N	number of inner iterations
RANS	Reynolds-Averaged Navier–Stokes
RBD	rigid-body dynamics
R_t	undamped eddy viscosity
y^+	nondimensional wall distance
α	angle of attack
k	turbulent kinetic energy
ε	dissipation rate
<u>Superscripts</u>	
B	body component
F	fin component
C	single-canard component

1 DEFENSE TECHNICAL
(PDF) INFORMATION CTR
DTIC OCA

2 DIRECTOR
(PDF) US ARMY RESEARCH LAB
RDRL CIO L
IMAL HRA MAIL & RECORDS
MGMT

1 GOVT PRINTG OFC
(PDF) A MALHOTRA

5 AMRDEC
(PDF) L AUMAN
J DOYLE
K KENNEDY
M MCDANIEL
C ROSEMA

6 ARDEC
(PDF) M STOLK
Y CHEN
T RECCHIA
D HOSIER
M DUCA
G RODEBAUGH

1 NWSCDD
(PDF) S KOSKI

1 USMA
(PDF) C VERHULST

27 DIR USARL
(PDF) RDRL WM
B FORCH
S KARNA
J LA SCALA
S SCHOENFELD
J ZABINSKI
RDRL WML
P PEREGINO
M ZOLTOSKI
RDRL WML A
W OBERLE
RDRL WML B
N TRIVEDI
RDRL WML C
S AUBERT
RDRL WML D
R BEYER
RDRL WML E
V BHAGWANDIN
I CELMINS
J DESPIRITO
F FRESCONI
J SAHU
P WEINACHT
RDRL WML F
T BROWN
M ILG
B KLINE
J MALEY
B NELSON
RDRL WML G
M MINNICINO
J SOUTH
RDRL WML H
J NEWILL
RDRL WMP
D LYON
RDRL WMS
H E MAUPIN